Spherical-earth Fréchet sensitivity kernels

Tarje Nissen-Meyer,[1] F. A. Dahlen[1] and Alexandre Fournier[2]

[1]*Department of Geosciences, Princeton University, Princeton,* NJ 08544, *USA. E-mail: tarje@princeton.edu*
[2]*Laboratoire de Géophysique Interne et Tectonophysique, Université Joseph Fourier,* 38041 *Grenoble Cedex* 9, *France*

SUMMARY
We outline a method that enables the efficient computation of exact Fréchet sensitivity kernels for a non-gravitating 3-D spherical earth model. The crux of the method is a 2-D weak formulation for determining the 3-D elastodynamic response of the earth model to both a moment-tensor and a point-force source. The sources are decomposed into their monopole, dipole and quadrupole constituents, with known azimuthal radiation patterns. The full 3-D response and, therefore, the 3-D waveform sensitivity kernel for an arbitrary source–receiver geometry, can be reconstructed from a series of six independent 2-D solutions, which may be obtained using a spectral-element or other mesh-based numerical method on a 2-D, planar, semicircular domain. This divide-and-conquer, 3-D to 2-D reduction strategy can be used to compute sensitivity kernels for any seismic phase, including grazing and diffracted waves, at relatively low computational cost.

Key words: Fréchet derivatives, global seismology, normal modes, numerical techniques, perturbation methods, seismic-wave propagation.

1 INTRODUCTION

Many features related to the thermal and chemical dynamics of the Earth's deep interior are the subject of ongoing seismological investigations, including the fine structure of the outer (e.g. Yu *et al.* 2005) and inner core (e.g. Ishii *et al.* 2002), the transition zone (Gu *et al.* 2003) and the core–mantle boundary region (e.g. Lay & Garnero 2004), ultralow velocity zones and deep partial melting (Lay *et al.* 2004), possible deep mantle stratification due to chemical reservoirs (Kellogg *et al.* 1999; Davaille 1999), strong anisotropy (Kendall 2000), deep mantle plumes (Montelli *et al.* 2004; Rost *et al.* 2005), and sharp vertical discontinuities bounding superplumes (To *et al.* 2005; Ni *et al.* 2005). Despite the ever-increasing resolution of seismic tomographic studies and a converging agreement on the presence of a thermo-chemical boundary layer in the D″ region (Lay & Garnero 2004), we are still at the dawn of constraining many lowermost mantle characteristics in terms of geodynamically critical unknowns such as the heat flux across the core–mantle boundary, the nature of mantle upwellings and downwellings, the scale lengths of 3-D heterogeneities and the interconnection between thermal, chemical, mineralogical and mechanical properties.

A number of recent and future developments show great promise for new and more detailed seismological insights into these regions, including software and hardware advances to model the propagation of seismic waves in realistic 3-D media, broadband digital seismic data, better path coverage by new seismometer locations (e.g. oceans, USArray) and improvements in the analytical treatment of both the seismic forward and inverse problem. To a large extent, global tomographic inversion still primarily relies on a small portion of the information present in a broadband seismogram, namely the traveltimes of direct and reflected body waves. While it is evident that the ultimate goal of seismic tomographers is to exploit all of the information present in seismic waveforms (e.g. Tarantola 1984), it has been argued that full-waveform inversion may easily fail even for weak 3-D velocity contrasts, due to the highly non-linear character of the misfit functions and the plethora of local minima limiting any gradient-based method (Gauthier *et al.* 1986). The relative merits of traveltime versus waveform inversion thus lie in the combined robustness and ease of computation, convergence and data selection. Aside from path coverage and other data-related discriminants, the physics underlying the inversion process plays a central role in recovering the Earth's 3-D structure. Correct expressions for the first-order sensitivity of a seismic waveform or cross-correlation traveltime have been known for more than two decades (Tarantola 1984; Luo & Schuster 1991; Woodward 1992), culminating more recently in the counter-intuitive observation that the traveltime sensitivity vanishes along the infinite-frequency ray path (Marquering *et al.* 1998; Dahlen *et al.* 2000). Further studies have addressed other aspects of the sensitivity of seismic waves, focusing upon body-wave amplitudes (Dahlen & Baig 2002), surface waves (Zhou *et al.* 2004), transversely isotropic media (Favier & Chevrot 2003), discontinuity undulations (Dahlen 2005), and approximate finite-frequency effects of diffracted and core phases (Hung *et al.* 2005). The determination of the exact sensitivity of a waveform to 3-D velocity and density
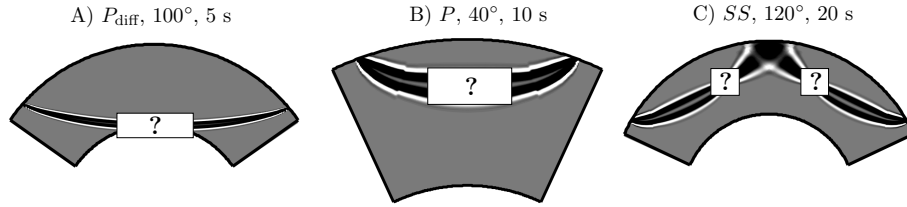
A) P_{diff}, 100°, 5 s   B) P, 40°, 10 s   C) SS, 120°, 20 s

Figure 1. Traveltime sensitivity kernels in PREM (Dziewonski & Anderson 1981), calculated using the ray-based approach of Dahlen *et al.* (2000). Question marks indicate regions where the sensitivity is not computed accurately due to the deficiencies of ray theory. (a) Sensitivity of a *P* wave grazing the core and emerging at an epicentral distance of 100°; the characteristic period is 5 s. An improved method is needed to compute the sensitivity in the D″ region. (b) Sensitivity of a 10 s *P* wave that propagates to an epicentral distance of 40°. Turning *P* and *S* waves at this distance and less are affected by upper-mantle triplications. (c) Sensitivity of a 20 s *SS* surface reflection that propagates to an epicentral distance of 120°. Question marks cover the source-to-receiver and receiver-to-source caustics, where ray theory incorrectly approximates the sensitivity. In all of these instances, the expectation is that the ray-based kernels will be an excellent approximation to the exact sensitivity kernels, except where covered by the question marks.

variations is a non-trivial computational problem, because it requires computation of the background-earth Green tensor and its spatial derivative at all relevant space and time points for all source–receiver configurations. Past attempts to calculate exact 3-D sensitivity kernels have been based upon spherical-earth normal-mode summation (Zhao *et al.* 2000; Capdeville 2005), finite differences (Zhao *et al.* 2005), and spectral-element simulations (Tromp *et al.* 2005). The latter study utilizes an innovative adjoint method (Tarantola 1984) to construct 3-D sensitivity kernels on-the-fly, requiring only two wave-propagation simulations for every earthquake. Although this idea is extremely promising in the long term, it is currently severely limited by computational resources, inasmuch as waveforms calculated on even the largest supercomputers resolve periods not much shorter than 5 s, and need to be recomputed for any change in the objective function or data set. The recent incorporation of finite-frequency effects into large-scale tomographic inversions (Montelli *et al.* 2004) makes use of approximate sensitivity kernels which rely upon seismic ray theory to approximate the Green tensor (Dahlen *et al.* 2000). Such ray-based Born sensitivity kernels are adequate for the non-triplicated, turning or reflected *P*, *S*, *PP*, *SS*, *PcP* and *ScS* waves inverted by Montelli *et al.* (2004); however, they are unable to account accurately for other phases, including near-grazing waves, core diffractions and upper-mantle triplications, that would be extremely useful in constraining global tomographic models. Fig. 1 shows ray-plane plots of three ray-based sensitivity kernels in PREM (Dziewonski & Anderson 1981), with question marks indicating regions where they are known to be inaccurately computed.

In this paper we describe a numerical scheme that enables the computation of exact 3-D sensitivity kernels for any portion of the seismic waveform in a background spherically symmetric earth. Because the scheme is limited to an unperturbed spherical earth, it cannot be used as the basis for iterative non-linear inversions like the adjoint method of Tromp *et al.* (2005). Its principal advantage over that fully 3-D method is the efficiency with which the kernels can be computed, even for high frequencies (>1 Hz), on a relatively small computer cluster. We achieve this improvement in efficiency by reducing the computation of the 3-D Green tensor to a series of equivalent 2-D problems. This divide-and-conquer strategy opens the door to storing a library of waveforms in 2-D to enable the computation of full 3-D Fréchet kernels for any given seismic phase, including core-grazing and core-diffracted waves, which can be used to improve tomographic imaging of heterogeneities in the lowermost mantle. In the paper following this one (Nissen-Meyer *et al.* 2007), we will introduce a numerical method based on 2-D spectral elements to compute the spherical-earth Green tensor and its spatial derivative.

2 FIRST-ORDER PERTURBATION THEORY

For simplicity, we ignore rotation, self-gravitation and anelasticity, and consider an unperturbed, anisotropic, elastic earth model occupying a finite volume $\oplus$ with surface $\partial\oplus$. Points within the model will be labelled by their position $\mathbf{r}$; we denote the mass density by $\rho(\mathbf{r})$ and the fourth-order elasticity tensor by $\mathbf{C}(\mathbf{r})$. The model is presumed to have a number of internal solid-solid discontinuities, the union of which is denoted by Σ_{SS}, and a number of internal fluid-solid discontinuities, the union of which is denoted by Σ_{FS}. The union of all the boundaries, including the outer free surface $\partial\oplus$, will be denoted by $\Sigma = \Sigma_{\text{SS}} \cup \Sigma_{\text{FS}} \cup \partial\oplus$. The unit outward normal to the composite surface Σ will be denoted by $\hat{\mathbf{n}}(\mathbf{r})$. In the fluid regions of the Earth, the components of the elasticity tensor $\mathbf{C}$ are given by $C_{ijkl} = \kappa \delta_{ij} \delta_{kl}$, where δ_{ij} is the Kronecker delta and $\kappa(\mathbf{r})$ is the isentropic incompressibility. In the solid regions $\mathbf{C}$ is constrained only by the customary elastic symmetry relations $C_{ijkl} = C_{jikl} = C_{ijlk} = C_{klij}$. We shall eventually, in Sections 3 and 4, limit consideration to an unperturbed earth model that is spherically symmetric, with an isotropic elasticity tensor of the form $C_{ijkl} = \lambda \delta_{ij} \delta_{kl} + \mu(\delta_{ik}\delta_{jl} + \delta_{il}\delta_{jk})$, where λ and μ are the Lamé parameters, related to the compressional and shear wave speeds v_{p} and v_{s} by $v_{\text{p}}^2 = (\lambda + 2\mu)/\rho$ and $v_{\text{s}}^2 = \mu/\rho$. In the present perturbation-theoretic discussion, however, there is no need to impose this restriction.

We denote the Green tensor of the unperturbed earth model by $\mathbf{G}(\mathbf{r}_{\text{r}}, t; \mathbf{r}_{\text{s}}, 0)$. By definition, $G_{pq}(\mathbf{r}_{\text{r}}, t; \mathbf{r}_{\text{s}}, 0)$ is the particle displacement measured in the pth direction at a receiver point $\mathbf{r}_{\text{r}}$ and time t, due to an impulsive force exerted in the qth direction at a source point $\mathbf{r}_{\text{s}}$ and time $t = 0$. The principle of source–receiver reciprocity guarantees that the Green tensor satisfies the relation (Aki & Richards 1980, Section 2.4; Dahlen & Tromp 1998, Section 4.1.7)

$$\mathbf{G}(\mathbf{r}_{\text{r}}, t; \mathbf{r}_{\text{s}}, 0) = \mathbf{G}^{\text{T}}(\mathbf{r}_{\text{s}}, t; \mathbf{r}_{\text{r}}, 0), \tag{1}$$

where the superscript T denotes the transpose, $G_{pq}^{\text{T}} = G_{qp}$.

Let $u(t)$ be the $\hat{\mathbf{p}}$ component of the displacement at the receiver $\mathbf{r}_r$ due to a step-function, moment-tensor source $\mathbf{M}H(t)$ situated at the source point $\mathbf{r}_s$. This moment-tensor response of the Earth is given in terms of the Green tensor by (Aki & Richards 1980, Section 3.3; Dahlen & Tromp 1998, Section 5.4.1)

$$u(t) = \int_0^t \mathbf{M} : \nabla_s \mathbf{G}^{\mathrm{T}}(\mathbf{r}_r, \tau; \mathbf{r}_s, 0) \cdot \hat{\mathbf{p}}\, d\tau, \tag{2}$$

where ∇_s denotes the gradient with respect to the source coordinates $\mathbf{r}_s$. For a more general earthquake source at $\mathbf{r}_s$, with a moment release history $m(t)$, $0 \le t \le \infty$, satisfying

$$\int_0^\infty \dot{m}(t)\, dt = 1, \tag{3}$$

where a dot denotes differentiation with respect to time, the displacement at $\mathbf{r}_r$ is given by

$$u(t) = \int_0^\infty \dot{m}(t - \tau) u_H(\tau)\, d\tau, \tag{4}$$

where $u_H(t)$ is the Heaviside response, given by eq. (2). We shall henceforth restrict attention to a step-function source $m(t) = H(t)$, and drop the subscript H upon the response $u(t)$.

2.1 Volumetric perturbation

Suppose now that the earth model is subjected to pointwise infinitesimal perturbations in the density and elastic properties, $\rho(\mathbf{r}) \to \rho(\mathbf{r}) + \delta\rho(\mathbf{r})$ and $\mathbf{C}(\mathbf{r}) \to \mathbf{C}(\mathbf{r}) + \delta\mathbf{C}(\mathbf{r})$. The moment-tensor response is altered as a result of this slight perturbation, $u(t) \to u(t) + \delta u(t)$. The Born approximation provides an explicit linear relation between the waveform perturbation $\delta u(t)$ and the volumetric model perturbations $\delta\rho(\mathbf{r})$ and $\delta\mathbf{C}(\mathbf{r})$. We do not provide an independent derivation of this well-known relationship (e.g. Chapman 2004, Section 10.3.1.2), but instead simply quote the result here. Two unperturbed displacement fields are required at every volumetric 'scatterer' location $\mathbf{r}$: the first is the response

$$\vec{\mathbf{u}}(\mathbf{r}, t) = \int_0^t \mathbf{M} : \nabla_s \mathbf{G}^{\mathrm{T}}(\mathbf{r}, \tau; \mathbf{r}_s, 0)\, d\tau \tag{5}$$

to the earthquake $\mathbf{M}H(t)$ situated at the source location $\mathbf{r}_s$, and the second is the response

$$\overleftarrow{\mathbf{u}}(\mathbf{r}, t) = \mathbf{G}(\mathbf{r}, t; \mathbf{r}_r, 0) \cdot \hat{\mathbf{p}}. \tag{6}$$

to an impulsive point force $\hat{\mathbf{p}}\,\delta(t)$ exerted in the receiver polarization direction at $\mathbf{r}_r$. Differentiation with respect to t and $\mathbf{r}$ yields the associated displacement and strain fields

$$\vec{\mathbf{v}}(\mathbf{r}, t) = \partial_t \vec{\mathbf{u}}(\mathbf{r}, t), \qquad \vec{\mathbf{E}}(\mathbf{r}, t) = \tfrac{1}{2}\left[\nabla \vec{\mathbf{u}}(\mathbf{r}, t) + \nabla \vec{\mathbf{u}}(\mathbf{r}, t)^{\mathrm{T}}\right], \tag{7}$$

$$\overleftarrow{\mathbf{v}}(\mathbf{r}, t) = \partial_t \overleftarrow{\mathbf{u}}(\mathbf{r}, t), \qquad \overleftarrow{\mathbf{E}}(\mathbf{r}, t) = \tfrac{1}{2}\left[\nabla \overleftarrow{\mathbf{u}}(\mathbf{r}, t) + \nabla \overleftarrow{\mathbf{u}}(\mathbf{r}, t)^{\mathrm{T}}\right]. \tag{8}$$

The forward-pointing and backward-pointing arrows serve as a mnemonic reminder that the fields $\vec{\mathbf{u}}$, $\vec{\mathbf{v}}$ and $\vec{\mathbf{E}}$ are considered to propagate in the forward direction from $\mathbf{r}_s$ to $\mathbf{r}$, whereas $\overleftarrow{\mathbf{u}}$, $\overleftarrow{\mathbf{v}}$ and $\overleftarrow{\mathbf{E}}$ are considered to propagate in the backward direction from $\mathbf{r}_r$ to $\mathbf{r}$. The perturbation $\delta u(t)$ is given in terms of $\delta\rho(\mathbf{r})$ and $\delta\mathbf{C}(\mathbf{r})$ by (Chapman 2004, eq. 10.3.42)

$$\delta u(t) = -\int_\oplus d^3\mathbf{r}\, \delta\rho(\mathbf{r}) \int_0^t \vec{\mathbf{v}}(\mathbf{r}, \tau) \cdot \overleftarrow{\mathbf{v}}(\mathbf{r}, t - \tau)\, d\tau - \int_\oplus d^3\mathbf{r} \int_0^t \vec{\mathbf{E}}(\mathbf{r}, \tau) : \delta\mathbf{C}(\mathbf{r}) : \overleftarrow{\mathbf{E}}(\mathbf{r}, t - \tau)\, d\tau. \tag{9}$$

Making use of an obvious index notation and suppressing all of the dependencies, we can rewrite this in the abbreviated form

$$\delta u = -\int_\oplus \left[\delta\rho\, \vec{v}_i * \overleftarrow{v}_i + \delta C_{ijkl}\, \vec{E}_{ij} * \overleftarrow{E}_{kl}\right] d^3\mathbf{r}, \tag{10}$$

where $*$ denotes time-domain convolution. The physical signal $u(t) + \delta u(t)$ propagates entirely in the forward direction, from the source $\mathbf{r}_s$ to the scatterer $\mathbf{r}$ and then to the receiver $\mathbf{r}_r$. We have made use of the reciprocity relation (1) to express the results (9) and (10) in terms of the backward-propagating velocity $\overleftarrow{\mathbf{v}} = \overleftarrow{v}_i\,\hat{\mathbf{x}}_i$ and strain $\overleftarrow{\mathbf{E}} = \overleftarrow{E}_{kl}\,\hat{\mathbf{x}}_k\hat{\mathbf{x}}_l$ at the scatterer $\mathbf{r}$.

2.2 Boundary perturbation

Suppose next that, in addition to the volumetric perturbations $\delta\rho$ and $\delta\mathbf{C}$, the boundary Σ is displaced outward (i.e. in the $\hat{\mathbf{n}}$ direction) by an infinitesimal amount $\delta d(\mathbf{r})$. In that case, eq. (10) must be supplemented by a boundary integral term (Dahlen 2005):

$$\delta u = -\int_\oplus \left[\delta\rho\, \vec{v}_i * \overleftarrow{v}_i + \delta C_{ijkl}\, \vec{E}_{ij} * \overleftarrow{E}_{kl}\right] d^3\mathbf{r}$$

$$+ \int_\Sigma \delta d\left[\rho\, \vec{v}_i * \overleftarrow{v}_i + C_{ijkl}\, \vec{E}_{ij} * \overleftarrow{E}_{kl} - n_i C_{ijkl}\, \overleftarrow{E}_{kl} * \partial_n \vec{u}_j - n_i C_{ijkl}\, \vec{E}_{kl} * \partial_n \overleftarrow{u}_j\right]_-^+ d^2\mathbf{r}$$

$$- \int_{\Sigma_{FS}} \delta d\left[n_i n_j C_{ijkl}\, \overleftarrow{E}_{kl} * \partial_q^\Sigma \vec{u}_q + n_i n_j C_{ijkl}\, \vec{E}_{kl} * \partial_q^\Sigma \overleftarrow{u}_q + \vec{u}_q * \partial_q^\Sigma(n_i n_j C_{ijkl}\, \overleftarrow{E}_{kl}) + \overleftarrow{u}_q * \partial_q^\Sigma(n_i n_j C_{ijkl}\, \vec{E}_{kl})\right]_-^+ d^2\mathbf{r}, \tag{11}$$
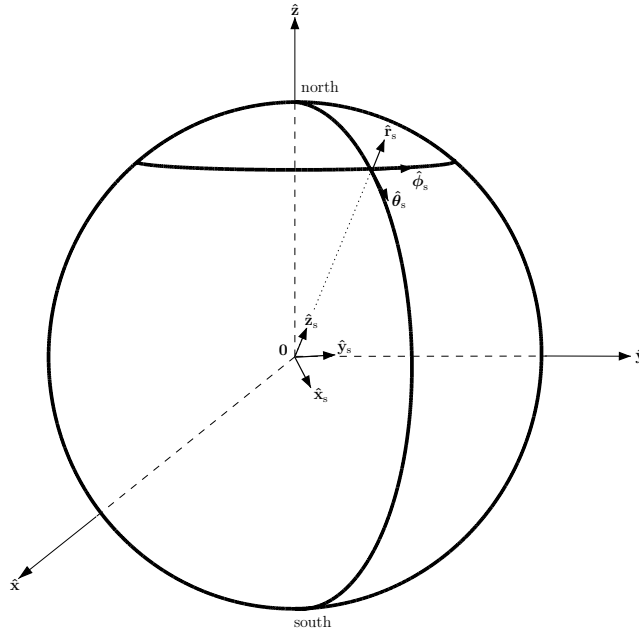
Figure 2. The transformation from source-centred to global coordinates. The Cartesian axes $\hat{\mathbf{x}}_s$, $\hat{\mathbf{y}}_s$, $\hat{\mathbf{z}}_s$ have their origin at the centre of the Earth, $\mathbf{r} = \mathbf{0}$, and are aligned with $\hat{\boldsymbol{\theta}}_s$, $\hat{\boldsymbol{\phi}}_s$, $\hat{\mathbf{r}}_s$, so that they point south, east and up, when parallel-transported to the source point, $\mathbf{r} = \mathbf{r}_s$. These source-centred axes are rotated to the global Greenwich axes $\hat{\mathbf{x}}$, $\hat{\mathbf{y}}$, $\hat{\mathbf{z}}$ by a matrix R_s. A similar rotation convention applies to the receiver point $\mathbf{r}_r$.

where $[\cdot]_-^+$ denotes the jump discontinuity in the enclosed quantity, upon going from the outside of the boundary Σ to the inside, and $\nabla^\Sigma = \hat{\mathbf{x}}_q \partial_q^\Sigma$ is the tangential gradient operator on Σ, defined by $\nabla = \hat{\mathbf{n}}\partial_n + \nabla^\Sigma$ (Woodhouse & Dahlen 1978; Dahlen & Tromp 1998, Section 13.1.6). It is noteworthy that the final integral in eq. (11) is only over the fluid-solid boundaries Σ_{FS}.

2.3 Rotation to the pole

In summary, two fundamental ingredients or building blocks are needed to compute a first-order waveform perturbation $\delta u(t)$, in the Born approximation:

(i) the forward-propagating displacement $\vec{\mathbf{u}}(\mathbf{r}, t)$ and associated velocity $\vec{\mathbf{v}}(\mathbf{r}, t)$ and strain $\vec{\mathbf{E}}(\mathbf{r}, t)$ generated in the unperturbed earth by a moment-tensor source $\mathbf{M}H(t)\delta(\mathbf{r} - \mathbf{r}_s)$,

(ii) the backward-propagating displacement $\overleftarrow{\mathbf{u}}(\mathbf{r}, t)$ and associated velocity $\overleftarrow{\mathbf{v}}(\mathbf{r}, t)$ and strain $\overleftarrow{\mathbf{E}}(\mathbf{r}, t)$ generated in the unperturbed earth by an impulsive point force $\hat{\mathbf{p}}\,\delta(t)\delta(\mathbf{r} - \mathbf{r}_r)$.

In the method to be described in this paper, the unperturbed, forward-propagating and backward-propagating responses are computed using independent systems of coordinates, in which the source $\mathbf{r}_s$ and the receiver $\mathbf{r}_r$, respectively, have been rotated so that they lie on or beneath the north pole. We discuss the geometrical considerations needed to transform the computed quantities to a global (Greenwich) coordinate system in this section. We take the origin $\mathbf{r} = \mathbf{0}$ to be at the centre of mass of the Earth, and denote the global Cartesian axes by $\hat{\mathbf{x}}$, $\hat{\mathbf{y}}$, $\hat{\mathbf{z}}$, and the spherical polar coordinates of the source and receiver by $\mathbf{r}_s = (r_s, \theta_s, \phi_s)$ and $\mathbf{r}_r = (r_r, \theta_r, \phi_r)$. Source coordinate axes $\hat{\mathbf{x}}_s$, $\hat{\mathbf{y}}_s$, $\hat{\mathbf{z}}_s$ are affixed to the origin $\mathbf{0}$, but are oriented so that they point south, east and up (i.e. in the $\hat{\boldsymbol{\theta}}_s$, $\hat{\boldsymbol{\phi}}_s$, $\hat{\mathbf{r}}_s$ directions) when parallel-transported to $\mathbf{r}_s$, as illustrated in Fig. 2. Receiver coordinate axes $\hat{\mathbf{x}}_r$, $\hat{\mathbf{y}}_r$, $\hat{\mathbf{z}}_r$ are likewise oriented so that they coincide with $\hat{\boldsymbol{\theta}}_r$, $\hat{\boldsymbol{\phi}}_r$, $\hat{\mathbf{r}}_r$ when parallel-transported to $\mathbf{r}_r$. The global, source and receiver coordinates of an arbitrary scatterer,

$$\mathbf{r} = x\hat{\mathbf{x}} + y\hat{\mathbf{y}} + z\hat{\mathbf{z}} = x_s\hat{\mathbf{x}}_s + y_s\hat{\mathbf{y}}_s + z_s\hat{\mathbf{z}}_s = x_r\hat{\mathbf{x}}_r + y_r\hat{\mathbf{y}}_r + z_r\hat{\mathbf{z}}_r, \tag{12}$$

are related by

$$\begin{pmatrix} x_s \\ y_s \\ z_s \end{pmatrix} = \mathsf{R}_s^{\mathsf{T}} \begin{pmatrix} x \\ y \\ z \end{pmatrix}, \qquad \begin{pmatrix} x_r \\ y_r \\ z_r \end{pmatrix} = \mathsf{R}_r^{\mathsf{T}} \begin{pmatrix} x \\ y \\ z \end{pmatrix}, \tag{13}$$

where the superscript T denotes the matrix transpose, and where

$$\mathsf{R}_s = \begin{pmatrix} \hat{\mathbf{x}}_s \cdot \hat{\mathbf{x}} & \hat{\mathbf{y}}_s \cdot \hat{\mathbf{x}} & \hat{\mathbf{z}}_s \cdot \hat{\mathbf{x}} \\ \hat{\mathbf{x}}_s \cdot \hat{\mathbf{y}} & \hat{\mathbf{y}}_s \cdot \hat{\mathbf{y}} & \hat{\mathbf{z}}_s \cdot \hat{\mathbf{y}} \\ \hat{\mathbf{x}}_s \cdot \hat{\mathbf{z}} & \hat{\mathbf{y}}_s \cdot \hat{\mathbf{z}} & \hat{\mathbf{z}}_s \cdot \hat{\mathbf{z}} \end{pmatrix} = \begin{pmatrix} \cos\theta_s \cos\phi_s & -\sin\phi_s & \sin\theta_s \cos\phi_s \\ \cos\theta_s \sin\phi_s & \cos\phi_s & \sin\theta_s \sin\phi_s \\ -\sin\theta_s & 0 & \cos\theta_s \end{pmatrix} \tag{14}$$

and

$$R_r = \begin{pmatrix} \hat{x}_r \cdot \hat{x} & \hat{y}_r \cdot \hat{x} & \hat{z}_r \cdot \hat{x} \\ \hat{x}_r \cdot \hat{y} & \hat{y}_r \cdot \hat{y} & \hat{z}_r \cdot \hat{y} \\ \hat{x}_r \cdot \hat{z} & \hat{y}_r \cdot \hat{z} & \hat{z}_r \cdot \hat{z} \end{pmatrix} = \begin{pmatrix} \cos\theta_r \cos\phi_r & -\sin\phi_r & \sin\theta_r \cos\phi_r \\ \cos\theta_r \sin\phi_r & \cos\phi_r & \sin\theta_r \sin\phi_r \\ -\sin\theta_r & 0 & \cos\theta_r \end{pmatrix} \tag{15}$$

are the rotation matrices that rotate the source $\mathbf{r}_s$ and the receiver $\mathbf{r}_r$ to the north pole.

Suppose we have the capability of computing the components

$$\vec{v}_s = \begin{pmatrix} \hat{x}_s \cdot \vec{v} \\ \hat{y}_s \cdot \vec{v} \\ \hat{z}_s \cdot \vec{v} \end{pmatrix}, \qquad \vec{E}_s = \begin{pmatrix} \hat{x}_s \cdot \vec{E} \cdot \hat{x}_s & \hat{x}_s \cdot \vec{E} \cdot \hat{y}_s & \hat{x}_s \cdot \vec{E} \cdot \hat{z}_s \\ \hat{y}_s \cdot \vec{E} \cdot \hat{x}_s & \hat{y}_s \cdot \vec{E} \cdot \hat{y}_s & \hat{y}_s \cdot \vec{E} \cdot \hat{z}_s \\ \hat{z}_s \cdot \vec{E} \cdot \hat{x}_s & \hat{z}_s \cdot \vec{E} \cdot \hat{y}_s & \hat{z}_s \cdot \vec{E} \cdot \hat{z}_s \end{pmatrix} \tag{16}$$

of the forward-propagating velocity and strain fields $\vec{v}(\mathbf{r}, t)$ and $\vec{E}(\mathbf{r}, t)$ in the source coordinate system $\hat{x}_s, \hat{y}_s, \hat{z}_s$. The corresponding components

$$\vec{v} = \begin{pmatrix} \hat{x} \cdot \vec{v} \\ \hat{y} \cdot \vec{v} \\ \hat{z} \cdot \vec{v} \end{pmatrix}, \qquad \vec{E} = \begin{pmatrix} \hat{x} \cdot \vec{E} \cdot \hat{x} & \hat{x} \cdot \vec{E} \cdot \hat{y} & \hat{x} \cdot \vec{E} \cdot \hat{z} \\ \hat{y} \cdot \vec{E} \cdot \hat{x} & \hat{y} \cdot \vec{E} \cdot \hat{y} & \hat{y} \cdot \vec{E} \cdot \hat{z} \\ \hat{z} \cdot \vec{E} \cdot \hat{x} & \hat{z} \cdot \vec{E} \cdot \hat{y} & \hat{z} \cdot \vec{E} \cdot \hat{z} \end{pmatrix} \tag{17}$$

in the global coordinate system $\hat{x}, \hat{y}, \hat{z}$ are given by the usual transformation relations

$$\vec{v} = R_s^T \vec{v}_s, \qquad \vec{E} = R_s^T \vec{E}_s R_s. \tag{18}$$

The receiver-coordinate components

$$\overleftarrow{v}_r = \begin{pmatrix} \hat{x}_r \cdot \overleftarrow{v} \\ \hat{y}_r \cdot \overleftarrow{v} \\ \hat{z}_r \cdot \overleftarrow{v} \end{pmatrix}, \qquad \overleftarrow{E}_r = \begin{pmatrix} \hat{x}_r \cdot \overleftarrow{E} \cdot \hat{x}_r & \hat{x}_r \cdot \overleftarrow{E} \cdot \hat{y}_r & \hat{x}_r \cdot \overleftarrow{E} \cdot \hat{z}_r \\ \hat{y}_r \cdot \overleftarrow{E} \cdot \hat{x}_r & \hat{y}_r \cdot \overleftarrow{E} \cdot \hat{y}_r & \hat{y}_r \cdot \overleftarrow{E} \cdot \hat{z}_r \\ \hat{z}_r \cdot \overleftarrow{E} \cdot \hat{x}_r & \hat{z}_r \cdot \overleftarrow{E} \cdot \hat{y}_r & \hat{z}_r \cdot \overleftarrow{E} \cdot \hat{z}_r \end{pmatrix} \tag{19}$$

of the backward-propagating velocity and strain fields $\overleftarrow{v}(\mathbf{r}, t)$ and $\overleftarrow{E}(\mathbf{r}, t)$ are likewise related to the global-coordinate components

$$\overleftarrow{v} = \begin{pmatrix} \hat{x} \cdot \overleftarrow{v} \\ \hat{y} \cdot \overleftarrow{v} \\ \hat{z} \cdot \overleftarrow{v} \end{pmatrix}, \qquad \overleftarrow{E} = \begin{pmatrix} \hat{x} \cdot \overleftarrow{E} \cdot \hat{x} & \hat{x} \cdot \overleftarrow{E} \cdot \hat{y} & \hat{x} \cdot \overleftarrow{E} \cdot \hat{z} \\ \hat{y} \cdot \overleftarrow{E} \cdot \hat{x} & \hat{y} \cdot \overleftarrow{E} \cdot \hat{y} & \hat{y} \cdot \overleftarrow{E} \cdot \hat{z} \\ \hat{z} \cdot \overleftarrow{E} \cdot \hat{x} & \hat{z} \cdot \overleftarrow{E} \cdot \hat{y} & \hat{z} \cdot \overleftarrow{E} \cdot \hat{z} \end{pmatrix} \tag{20}$$

by

$$\overleftarrow{v} = R_r^T \overleftarrow{v}_r, \qquad \overleftarrow{E} = R_r^T \overleftarrow{E}_r R_r. \tag{21}$$

2.4 Computational outline

To conclude this section, we outline the steps needed to compute a first-order waveform perturbation $\delta u(t)$:

(i) Compute the matrices R_s, R_r that rotate the source and receiver $\mathbf{r}_r$, $\mathbf{r}_s$ to the pole.
(ii) Find the source and receiver coordinates of a selected scatterer $\mathbf{r} = (x, y, z)$.
(iii) Compute the unperturbed, forward-propagating velocity $\vec{v}_s$ and strain $\vec{E}_s$.
(iv) Compute the unperturbed, backward-propagating velocity $\overleftarrow{v}_r$ and strain $\overleftarrow{E}_r$.
(v) Transform $\vec{v}_s$, $\vec{E}_s$ and $\overleftarrow{v}_r$, $\overleftarrow{E}_r$ to global coordinates $\vec{v}$, $\vec{E}$ and $\overleftarrow{v}$, $\overleftarrow{E}$.
(vi) Use $\vec{v}$, $\vec{E}$ and $\overleftarrow{v}$, $\overleftarrow{E}$ to compute the convolutions $-\delta\rho \, \vec{v}_i * \overleftarrow{v}_i - \delta C_{ijkl} \vec{E}_{ij} * \overleftarrow{E}_{kl}$.
(vii) Additional convolutions are required if there are also boundary perturbations δd.
(viii) Repeat for all scatterers $\mathbf{r}$ and integrate over $\oplus$ and Σ to find $\delta u(t)$.

Steps (iii) and (iv) are the crux of the calculation. Fundamentally, we need to be able to compute the forward-propagating displacement field $\vec{u}$ and its temporal and spatial derivatives $\vec{v}$, $\vec{E}$ in a system of coordinates with the source $\mathbf{r}_s$ rotated to the north pole, and the backward-propagating displacement field $\overleftarrow{u}$ and its temporal and spatial derivatives $\overleftarrow{v}$, $\overleftarrow{E}$ in a system of coordinates with the receiver $\mathbf{r}_s$ rotated to the north pole. A numerical scheme for conducting such calculations is, in fact, the central topic of this paper; so far, all we have done is articulate our principal motivation for developing such a scheme.

3 SNREI EARTH MODEL

We shall, in our numerical scheme, restrict attention to an unperturbed SNREI earth model, having spherical boundaries $\Sigma = \Sigma_{SS} \cup \Sigma_{FS} \cup \partial\oplus$, with unit normal everywhere equal to the radial vector, $\hat{n} = \hat{r}$. The density ρ, fluid incompressibility κ, solid Lamé parameters λ and μ,

and compressional and shear wave speeds v_p and v_s are all functions only of radius $r = \|\mathbf{r}\|$. The source $\mathbf{r}_s$ and receiver $\mathbf{r}_r$ will henceforth always be considered to lie on or beneath the north pole. The subscripts s and r will be dropped from the coordinate axes $\hat{\mathbf{x}}_s, \hat{\mathbf{y}}_s, \hat{\mathbf{z}}_s$ and $\hat{\mathbf{x}}_r, \hat{\mathbf{y}}_r, \hat{\mathbf{z}}_r$, for simplicity, and the spherical polar coordinates of an arbitrary scatterer will now be denoted simply by $\mathbf{r} = (r, \theta, \phi)$. The polar coordinates of the source and receiver are $\mathbf{r}_s = (r_s, 0, \cdot)$ and $\mathbf{r}_r = (r_r, 0, \cdot)$, where the dots are indicative of the indeterminateness of the longitude ϕ at the pole. In any realistic whole-earth application, the receiver will be situated on the free surface, so that $r_r = r_0$, the radius of the Earth. The earthquake moment tensor $\mathbf{M}$ and receiver polarization vector $\hat{\mathbf{p}}$ will be expressed in terms of their $\hat{\mathbf{x}}, \hat{\mathbf{y}}, \hat{\mathbf{z}}$ components in the form

$$\mathbf{M} = M_{xx}\hat{\mathbf{x}}\hat{\mathbf{x}} + M_{yy}\hat{\mathbf{y}}\hat{\mathbf{y}} + M_{zz}\hat{\mathbf{z}}\hat{\mathbf{z}} + M_{xy}(\hat{\mathbf{x}}\hat{\mathbf{y}} + \hat{\mathbf{y}}\hat{\mathbf{x}}) + M_{xz}(\hat{\mathbf{x}}\hat{\mathbf{z}} + \hat{\mathbf{z}}\hat{\mathbf{x}}) + M_{yz}(\hat{\mathbf{y}}\hat{\mathbf{z}} + \hat{\mathbf{z}}\hat{\mathbf{y}}),\tag{22}$$

$$\hat{\mathbf{p}} = p_x\hat{\mathbf{x}} + p_y\hat{\mathbf{y}} + p_z\hat{\mathbf{z}}.\tag{23}$$

In this notation, M_{xz} and M_{yz} correspond to $\hat{\boldsymbol{\theta}}_s \cdot \mathbf{M} \cdot \hat{\mathbf{r}}_s$ and $\hat{\boldsymbol{\phi}}_s \cdot \mathbf{M} \cdot \hat{\mathbf{r}}_s$ at the global source location $\mathbf{r}_s$, and p_x, p_y, p_z point to the south, east and up (i.e. in the $\hat{\boldsymbol{\theta}}_r, \hat{\boldsymbol{\phi}}_r$ and $\hat{\mathbf{r}}_r$ directions) at the global receiver location $\mathbf{r}_r$.

3.1 Mode-sum representation of the response

The response of a spherically symmetric, non-rotating, elastic earth model to a polar moment-tensor or point-force source $\mathbf{M}H(t)$ or $\hat{\mathbf{p}}\,\delta(t)$ can be expressed as a sum over the normal modes of free oscillation. We review this mode-sum representation of the response in what follows, since it provides a useful guide to the expected form of the alternative solution which we seek to develop. The results in this section are not restricted to a SNREI earth model, but are applicable to any elastic earth model that is invariant with respect to rigid rotations about its centre. We adopt the normal-mode nomenclature of Dahlen & Tromp (1998), denoting the eigenfrequency of a mode of angular degree $l = 0, 1, \ldots$ and overtone number $n = 0, 1, \ldots$ by ${}_n\omega_l$, and normalizing the associated spheroidal and toroidal eigenfunctions by

$$\int_0^{r_0} \left[{}_nU_l^2(r) + {}_nV_l^2(r) + {}_nW_l^2(r) \right] r^2\,dr = 1.\tag{24}$$

The forward-propagating response to a step-function moment-tensor source is of the form (Dahlen & Tromp 1998, eq. 4.67)

$$\vec{\mathbf{u}}\,(\mathbf{r}, t) = \sum_{n=0}^{\infty} \sum_{l=0}^{\infty} {}_n\omega_l^{-2}\, {}_n\vec{\mathbf{A}}_l\,(\mathbf{r})\left[1 - \cos({}_n\omega_l t)\right],\tag{25}$$

whereas the backward-propagating response to an impulsive point force is of the form (Dahlen & Tromp 1998, eq. 4.60)

$$\overleftarrow{\mathbf{u}}\,(\mathbf{r}, t) = \sum_{n=0}^{\infty} \sum_{l=0}^{\infty} {}_n\omega_l^{-1}\, {}_n\overleftarrow{\mathbf{A}}_l\,(\mathbf{r})\sin({}_n\omega_l t).\tag{26}$$

The vector amplitude factors ${}_n\vec{\mathbf{A}}_l(\mathbf{r})$ and ${}_n\overleftarrow{\mathbf{A}}_l(\mathbf{r})$ describing the shape of every spherical-earth oscillation are given by (Dahlen & Tromp 1998, eqs 10.52 and 10.60)

$$\overleftrightarrow{\mathbf{A}}(r, \theta, \phi) = \left(\frac{2l+1}{4\pi}\right)\left\{\hat{\mathbf{r}}U(r) + \hat{\boldsymbol{\theta}}k^{-1}\left[V(r)\partial_\theta + W(r)(\sin\theta)^{-1}\partial_\phi\right] + \hat{\boldsymbol{\phi}}k^{-1}\left[V(r)(\sin\theta)^{-1}\partial_\phi - W(r)\partial_\theta\right]\right\}\overleftrightarrow{A}\,(\theta, \phi),\tag{27}$$

where the double-sided arrows point in either direction, and where we have let $k = \sqrt{l(l+1)}$ and dropped the subscripts n and l for simplicity. The depth-independent, forward-propagating scalar ${}_n\vec{A}_l(\theta, \phi)$ is a sum over surface spherical harmonics of degree l and orders $0 \leq m \leq 2$ (Dahlen & Tromp 1998, eqs 10.53–10.59)

$$\vec{A} = a_0 P_{l0}(\cos\theta) + P_{l1}(\cos\theta)(a_1\cos\phi + b_1\sin\phi) + P_{l2}(\cos\theta)(a_2\cos 2\phi + b_2\sin 2\phi),\tag{28}$$

where

$$a_0 = M_{zz}\,U_s' + (M_{xx} + M_{yy})r_s^{-1}\left(U_s - \tfrac{1}{2}kV_s\right),\tag{29}$$

$$a_1 = k^{-1}[M_{xz}(V_s' - r_s^{-1}V_s + kr_s^{-1}U_s) - M_{yz}(W_s' - r_s^{-1}W_s)],\tag{30}$$

$$b_1 = k^{-1}[M_{yz}(V_s' - r_s^{-1}V_s + kr_s^{-1}U_s) + M_{xz}(W_s' - r_s^{-1}W_s)],\tag{31}$$

$$a_2 = k^{-1}r_s^{-1}\left[\tfrac{1}{2}(M_{xx} - M_{yy})V_s - M_{xy}W_s\right],\tag{32}$$

$$b_2 = k^{-1}r_s^{-1}\left[M_{xy}V_s + \tfrac{1}{2}(M_{xx} - M_{yy})W_s\right].\tag{33}$$

The backward-propagating scalar $\overleftarrow{A}(\theta, \phi)$ has an analogous form, except that the order is restricted to $0 \leq m \leq 1$:

$$\overleftarrow{A} = c_0 P_{l0}(\cos\theta) + P_{l1}(\cos\theta)(c_1\cos\phi + d_1\sin\phi),\tag{34}$$

where

$$c_0 = p_z U_r, \qquad c_1 = k^{-1}\left(p_x V_r - p_y W_r\right), \qquad d_1 = k^{-1}\left(p_y V_r + p_x W_r\right).\tag{35}$$

A prime in eqs (29)–(33) denotes differentiation with respect to radius r, and the subscripts s and r denote evaluation of U, V and W at the source and receiver radii, $r = r_s$ and $r = r_r$. The quantities P_{l0}, P_{l1}, P_{l2} are the associated Legendre functions of degree l and orders $m = 0, 1, 2$ (e.g. Dahlen & Tromp 1998, eq. B.48).

3.2 Monopole, dipole and quadrupole sources

Inspection of the above results shows that the forward- and backward-propagating, spherical-earth responses $\vec{\mathbf{u}}(\mathbf{r}, t)$ and $\overleftarrow{\mathbf{u}}(\mathbf{r}, t)$ can be expressed as a linear superposition of three different types of sources, which can be distinguished on the basis of their azimuthal dependence on ϕ:

   (i) monopole sources, for which $\vec{\mathbf{u}}$ and $\overleftarrow{\mathbf{u}}$ are independent of ϕ,
   (ii) dipole sources, for which $\vec{\mathbf{u}}$ and $\overleftarrow{\mathbf{u}}$ vary as $\cos\phi$ or $\sin\phi$,
   (iii) quadrupole sources, for which $\vec{\mathbf{u}}$ and $\overleftarrow{\mathbf{u}}$ vary as $\cos 2\phi$ or $\sin 2\phi$.

The source-coordinate representation of the moment tensor $\mathbf{M}$ in eq. (22) can be rearranged to yield a representation of $\mathbf{M}$ in terms of its monopole, dipole and quadrupole constituents:

$$\mathbf{M} = \overbrace{M_{zz}\hat{\mathbf{z}}\hat{\mathbf{z}} + \tfrac{1}{2}(M_{xx} + M_{yy})(\hat{\mathbf{x}}\hat{\mathbf{x}} + \hat{\mathbf{y}}\hat{\mathbf{y}})}^{\text{monopole}} + \overbrace{M_{xz}(\hat{\mathbf{x}}\hat{\mathbf{z}} + \hat{\mathbf{z}}\hat{\mathbf{x}}) + M_{yz}(\hat{\mathbf{y}}\hat{\mathbf{z}} + \hat{\mathbf{z}}\hat{\mathbf{y}})}^{\text{dipole}}$$
$$+ \underbrace{\tfrac{1}{2}(M_{xx} - M_{yy})(\hat{\mathbf{x}}\hat{\mathbf{x}} - \hat{\mathbf{y}}\hat{\mathbf{y}}) + M_{xy}(\hat{\mathbf{x}}\hat{\mathbf{y}} + \hat{\mathbf{y}}\hat{\mathbf{x}})}_{\text{quadrupole}}. \tag{36}$$

Likewise, the point force (23) is a sum of monopole and dipole sources:

$$\hat{\mathbf{p}} = \underbrace{p_z\hat{\mathbf{z}}}_{\text{monopole}} + \underbrace{p_x\hat{\mathbf{x}} + p_y\hat{\mathbf{y}}}_{\text{dipole}}. \tag{37}$$

The dipole sources in eq. (36) as well as those in eq. (37) may be treated simultaneously, because the response $\vec{\mathbf{u}}$ to an M_{yz} source at longitude ϕ is identical to the response to an M_{xz} source at longitude $\phi - \pi/2$, and the response $\overleftarrow{\mathbf{u}}$ to a p_y source at longitude ϕ is identical to the response to a p_x source at longitude $\phi - \pi/2$. Likewise, the two quadrupole sources in eq. (36) may be treated simultaneously, since the response $\vec{\mathbf{u}}$ to an M_{xy} source at longitude ϕ is identical to the response to a $\tfrac{1}{2}(M_{xx} - M_{yy})$ source at longitude $\phi - \pi/4$. Altogether, we can reconstruct the full forward- and backward-propagating displacement fields $\vec{\mathbf{u}}(\mathbf{r}, t)$ and $\overleftarrow{\mathbf{u}}(\mathbf{r}, t)$ by considering six independent source types:

   (i) a p_z monopole source,
   (ii) an M_{zz} monopole source,
   (iii) a $\tfrac{1}{2}(M_{xx} + M_{yy})$ monopole source,
   (iv) a p_x or p_y dipole source,
   (v) an M_{xz} or M_{yz} dipole source,
   (vi) a $\tfrac{1}{2}(M_{xx} - M_{yy})$ or M_{xy} quadrupole source.

We describe the preliminaries of a numerical scheme for solving these six types of source problems within a SNREI earth in the next section. The essential strategy is to effect a reduction in the dimension from 3-D to 2-D by accounting explicitly for the known azimuthal dependence of the responses $\vec{\mathbf{u}}(\mathbf{r}, t)$ or $\overleftarrow{\mathbf{u}}(\mathbf{r}, t)$ to a monopole, dipole or quadrupole source. The resulting 2-D integral equations can be solved numerically within a D-shaped, planar, semicircular disk, as illustrated schematically in Fig. 3. The method we describe can be generalised to a transversely isotropic, spherically symmetric earth model such as PREM (Dziewonski & Anderson 1981).

4 REDUCED-DIMENSION WEAK FORMULATION

In what follows, we shall be obliged to pay closer attention to the distinction between the fluid and solid regions of the Earth than we have done so far; to that end, we introduce some refinements in our notation. For simplicity, we shall restrict attention to SNREI earth models with a solid inner core, overlain by a fluid outer core, overlain by a solid mantle and crust, but with no surficial ocean. We shall henceforth use three-letter symbols to label the various regions and the spherical boundaries that separate them:

   SIC: solid inner core,
   FOC: fluid outer core,
   SMC: solid mantle-plus-crust,
   ICB: inner-core boundary,
   CMB: core–mantle boundary.

We shall also de-emphasize the distinction between the forward-propagating, moment-tensor and backward-propagating, point-force responses, using generic, arrowless symbols $\mathbf{u}$, $\mathbf{E}$, $\mathbf{T}$ to refer to the displacements, strains and stresses $\vec{\mathbf{u}}, \vec{\mathbf{E}}, \vec{\mathbf{T}}$ and $\overleftarrow{\mathbf{u}}, \overleftarrow{\mathbf{E}}, \overleftarrow{\mathbf{T}}$.

4.1 Equations of motion

To find $\mathbf{u}(\mathbf{r}, t)$ everywhere within the Earth, we must solve the usual strong form of the equations of motion,

$$\rho\partial_t^2\mathbf{u} = \nabla\cdot\mathbf{T} \quad \text{in SIC}, \tag{38}$$

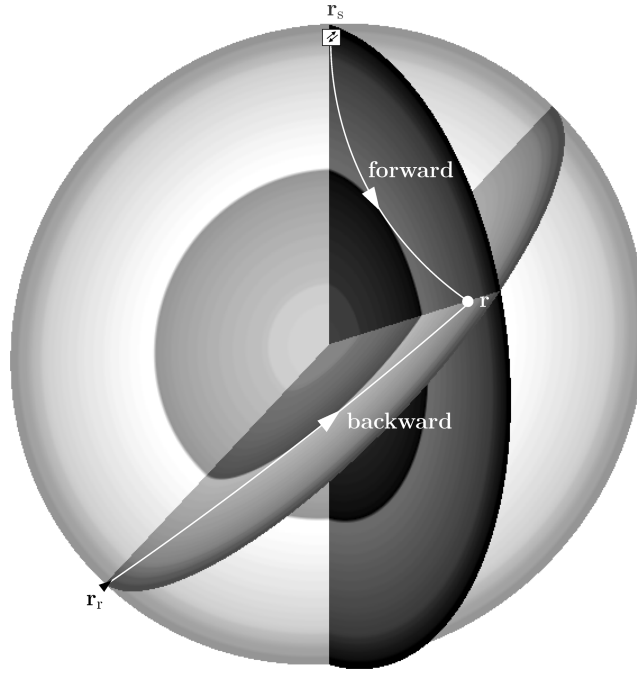$$\rho\partial_t^2\mathbf{u} = -\nabla P \quad \text{in FOC}, \tag{39}$$

Figure 3. Sketch illustrating the 2-D computation of the 3-D forward- and backward-propagating responses at an arbitrary scatterer $\mathbf{r}$. The points $\mathbf{r}_s$ and $\mathbf{r}_r$ are the locations of the source and receiver, where waves are excited by a moment tensor $\mathbf{M}H(t)$ and a point force $\hat{\mathbf{p}}\,\delta(t)$, respectively. Shading is suggestive of the radial velocity variation within the spherically symmetric model, with a solid inner core and fluid outer core, overlain by a solid mantle and crust. Numerical computation of the forward- and backward-propagating wavefields is conducted within the two intersecting, semicircular 2-D domains, denoted by the darker shading. The full 3-D moment-tensor and point-force responses can be reconstructed from six 2-D solutions, due to the known azimuthal dependence of the wavefields in a spherically symmetric earth.

$$\rho\partial_t^2\mathbf{u} = \nabla\cdot\mathbf{T} + \left\{\begin{array}{c}\hat{\mathbf{p}}\,\delta(\mathbf{r}-r_r\hat{\mathbf{z}})\,\delta(t) \\ -\mathbf{M}\cdot\nabla\delta(\mathbf{r}-r_s\hat{\mathbf{z}})\,H(t)\end{array}\right\} \quad\text{in SMC,} \tag{40}$$

subject to the kinematical and dynamical boundary conditions that

$$[\hat{\mathbf{r}}\cdot\mathbf{u}]_-^+ = 0 \quad\text{and}\quad \hat{\mathbf{r}}\cdot\mathbf{T} = -\hat{\mathbf{r}}P \quad\text{on ICB and CMB,} \tag{41}$$

and that $\hat{\mathbf{r}}\cdot\mathbf{T} = \mathbf{0}$ on the free outer surface $\partial\oplus$. The solid stress $\mathbf{T}(\mathbf{r},t)$ and the dynamical fluid pressure $P(\mathbf{r},t)$ are given by

$$\mathbf{T} = \lambda(\nabla\cdot\mathbf{u})\mathbf{I} + 2\mu\mathbf{E} \quad\text{in SIC and SMC,} \tag{42}$$

$$P = -\kappa(\nabla\cdot\mathbf{u}) \quad\text{in FOC.} \tag{43}$$

We shall continue to use $\lambda(r)$ and $\mu(r)$ to denote the Lamé parameters within SIC and SMC, and $\kappa(r)$ to denote the incompressibility within FOC.

4.2 Potential formulation in the fluid core

Following Komatitsch *et al.* (2000), Komatitsch & Tromp (2002) and Chaljub & Valette (2004) we shall find it convenient to adopt a potential formulation within the fluid core. Specifically, we write the displacement $\mathbf{u}(\mathbf{r},t)$ and the pressure $P(\mathbf{r},t)$ in terms of a potential $\chi(\mathbf{r},t)$ in the form (Chaljub & Valette 2004)

$$\mathbf{u} = \rho^{-1}\nabla\chi, \quad P = -\partial_t^2\chi. \tag{44}$$

Upon substituting the representations (44) into eq. (39), we obtain a second-order differential equation for the potential $\chi(\mathbf{r},t)$:

$$\kappa^{-1}\partial_t^2\chi = \nabla\cdot(\rho^{-1}\nabla\chi) \quad\text{in FOC.} \tag{45}$$

The fluid-solid boundary conditions (41) reduce to

$$\hat{\mathbf{r}}\cdot\mathbf{u} = \rho^{-1}\partial_r\chi \quad\text{and}\quad \hat{\mathbf{r}}\cdot\mathbf{T} = \hat{\mathbf{r}}\partial_t^2\chi \quad\text{on ICB and CMB.} \tag{46}$$

The completeness of the potential representation (44) is guaranteed by the absence of toroidal motion within an inviscid fluid core.

4.3 3-D weak formulation

To derive the integral or weak form of the above equations of motion, we dot eqs (38) and (40) with a test vector $\mathbf{w}$ ($\mathbf{r}$), multiply eq. (45) by a test scalar $w(\mathbf{r})$, and integrate by parts over the 3-D earth $\oplus$, making use of the fluid-solid boundary conditions (46) and the free-surface condition $\hat{\mathbf{r}} \cdot \mathbf{T} = \mathbf{0}$ on $\partial\oplus$. A solution $\mathbf{u}$, χ in an appropriate space with square-integrable derivatives is then sought such that, for all admissible $\mathbf{w}$, w, the following three integral equalities (obtained after integration over SIC, FOC and SMC) hold in the order listed below:

$$\int_{\text{SIC}} \left[\rho \mathbf{w} \cdot \partial_t^2 \mathbf{u} + \lambda (\nabla \cdot \mathbf{w})(\nabla \cdot \mathbf{u}) + 2\mu \nabla \mathbf{w} : \mathbf{E} \right] d^3\mathbf{r} - \int_{\text{ICB}} (\hat{\mathbf{r}} \cdot \mathbf{w}) \partial_t^2 \chi \, d^2\mathbf{r} = 0, \tag{47}$$

$$\int_{\text{FOC}} \left[\kappa^{-1} w \partial_t^2 \chi + \rho^{-1} \nabla w \cdot \nabla \chi \right] d^3\mathbf{r} + \int_{\text{ICB}} w(\hat{\mathbf{r}} \cdot \mathbf{u}) \, d^2\mathbf{r} - \int_{\text{CMB}} w(\hat{\mathbf{r}} \cdot \mathbf{u}) \, d^2\mathbf{r} = 0, \tag{48}$$

$$\int_{\text{SMC}} \left[\rho \mathbf{w} \cdot \partial_t^2 \mathbf{u} + \lambda (\nabla \cdot \mathbf{w})(\nabla \cdot \mathbf{u}) + 2\mu \nabla \mathbf{w} : \mathbf{E} \right] d^3\mathbf{r} + \int_{\text{CMB}} (\hat{\mathbf{r}} \cdot \mathbf{w}) \partial_t^2 \chi \, d^2\mathbf{r} = \left\{ \begin{array}{c} \hat{\mathbf{p}} \cdot \mathbf{w}(r_r \hat{\mathbf{z}}) \, \delta(t) \\ \mathbf{M} : \nabla \mathbf{w}(r_s \hat{\mathbf{z}}) \, H(t) \end{array} \right\}. \tag{49}$$

The SIC, FOC and SMC eqs (47)–(49) are coupled by virtue of the boundary integrals over ICB and CMB. It is noteworthy that the source terms on the right side of eq. (49) only involve the test vector $\mathbf{w}(r_r \hat{\mathbf{z}})$ and its gradient $\nabla \mathbf{w}(r_s \hat{\mathbf{z}})$ evaluated at the polar receiver and earthquake locations. Eqs (47)–(49) are identical to eqs (24), (23) and (16) of Komatitsch & Tromp (2002), except that they used a velocity potential representation $\mathbf{v} = \partial_t \mathbf{u} = -\rho^{-1} \nabla \chi$, $P = \partial_t \chi$ rather than the displacement potential representation (44), first introduced by Chaljub & Valette (2004).

4.4 2-D computational domain

Our objective in the remainder of this paper is to reduce the 3-D weak formulation (47)–(49) to a collection of 2-D weak problems, one for each of the six source types listed in Section 3.2. The computational domain for each of these problems is a planar, D-shaped region Ω, with a boundary $\partial\Omega$ consisting of a straight left edge corresponding to the polar axis, and a semicircular boundary on the right corresponding to the free surface of the 3-D earth, as illustrated in Fig. 4. We shall continue to refer to the various solid and fluid subdomains by SIC, FOC and SMC, and to the semicircular boundaries separating them as ICB and CMB. Following Bernardi *et al.* (1999), Gerritsma & Phillips (2000) and Fournier *et al.* (2004, 2005) we shall employ a system of cylindrical polar coordinates s, z related to the spherical polar coordinates in eqs (27)–(28) by

$$s = r \sin\theta, \quad z = r \cos\theta, \quad r = \sqrt{s^2 + z^2}, \quad \theta = \left\{ \begin{array}{ll} \arctan(s/z) & \text{if } z \geq 0, \\ \arctan(s/z) + \pi & \text{if } z < 0, \end{array} \right. \tag{50}$$

The unit vectors $\hat{\mathbf{s}}$, $\hat{\mathbf{z}}$ are Cartesian axes within the 2-D computational domain $\Omega = \text{SIC} \cup \text{FOC} \cup \text{SMC}$, with an origin $\mathbf{0}$ at the centre of the Earth. The unit radial vector on ICB and CMB is given by

$$\hat{\mathbf{r}} = \hat{\mathbf{s}} \sin\theta + \hat{\mathbf{z}} \cos\theta = \frac{s\hat{\mathbf{s}} + z\hat{\mathbf{z}}}{\sqrt{s^2 + z^2}}. \tag{51}$$

We consider monopole, dipole and quadrupole sources separately, in the next three sections.

4.5 Monopole source

Inspection of the mode-sum eqs (25)–(35) shows that the response $\mathbf{u}$ ($\mathbf{r}$, t), $\chi(\mathbf{r}, t)$ to a p_z, M_{zz} or $\frac{1}{2}(M_{xx} + M_{yy})$ monopole source is of the form

$$\mathbf{u} = \hat{\mathbf{s}} u_s(s, z, t) + \hat{\mathbf{z}} u_z(s, z, t), \quad \chi = \chi(s, z, t). \tag{52}$$

We choose time-independent test functions $\mathbf{w}(\mathbf{r})$, $w(\mathbf{r})$ of the same form, i.e.

$$\mathbf{w} = \hat{\mathbf{s}} w_s(s, z) + \hat{\mathbf{z}} w_z(s, z), \quad w = w(s, z). \tag{53}$$

To reduce the dimensionality of the weak formulation (47)–(49), we substitute the monopole representations (52)–(53), employ the cylindrical polar formula for the gradient operator, $\nabla = \hat{\mathbf{s}} \partial_s + \hat{\mathbf{z}} \partial_z + \hat{\boldsymbol{\phi}} s^{-1} \partial_\phi$, and the cylindrical divergence operator, $\nabla \cdot \mathbf{u} = (\partial_s + s^{-1}) u_s + s^{-1} \partial_\phi u_\phi + \partial_z u_z$, and evaluate the integrals $\int_0^{2\pi} d\phi = 2\pi$ over the longitude ϕ. This yields a 2-D system of weak equations governing the three unknowns $u_s(s, z, t)$, $u_z(s, z, t)$ and $\chi(s, z, t)$, which are equivalent to the 3-D system (47)–(49):

$$\int_{\text{SIC}} \left[\rho(w_s \partial_t^2 u_s + w_z \partial_t^2 u_z) + \lambda(\partial_s w_s + \partial_z w_z + s^{-1} w_s)(\partial_s u_s + \partial_z u_z + s^{-1} u_s) \right.$$

$$\left. + 2\mu(\partial_s w_s \partial_s u_s + \partial_z w_z \partial_z u_z + s^{-2} w_s u_s) + \mu(\partial_s w_z + \partial_z w_s)(\partial_s u_z + \partial_z u_s) \right] s \, ds \, dz$$

$$- \int_{\text{ICB}} \left(\frac{s w_s + z w_z}{\sqrt{s^2 + z^2}} \right) \partial_t^2 \chi \, s \, ds \, dz = 0, \tag{54}$$
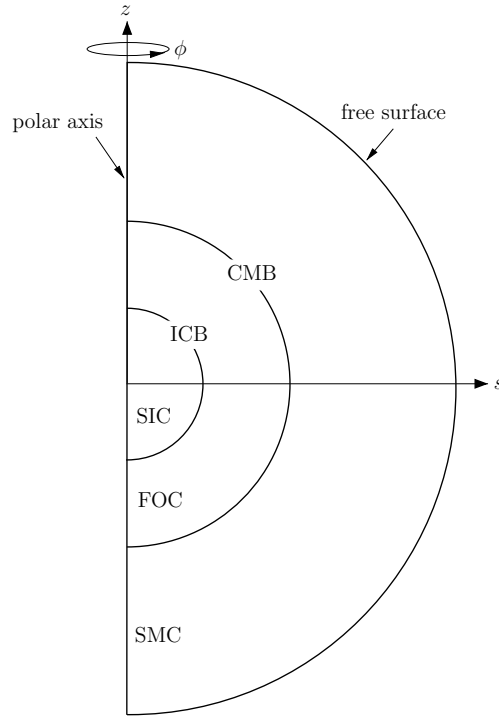
Figure 4. Planar 2-D computational domain Ω composed of the subdomains SIC, FOC and SMC, with intervening fluid-solid boundaries ICB and CMB; the cylindrical coordinates s, ϕ, z are indicated. The outer boundary $\partial\Omega$ consists of two portions, a semicircular arc on the right corresponding to the free surface, where the boundary condition $\hat{\mathbf{r}} \cdot \mathbf{T} = \mathbf{0}$ is automatically satisfied in the weak formulation, and a straight left edge, corresponding to the polar axis passing through the 3-D earth. Special attention must be paid to this axis, because of the presence of divergent factors such as s^{-1} and s^{-2} in the governing 2-D integral eqs (54)–(56), (61)–(63) and (69)–(71).

$$\int_{\text{FOC}} \left[\kappa^{-1} w \partial_t^2 \chi + \rho^{-1}(\partial_s w \partial_s \chi + \partial_z w \partial_z \chi)\right] s \, ds \, dz$$

$$+ \int_{\text{ICB}} w\left(\frac{s u_s + z u_z}{\sqrt{s^2 + z^2}}\right) s \, ds \, dz - \int_{\text{CMB}} w\left(\frac{s u_s + z u_z}{\sqrt{s^2 + z^2}}\right) s \, ds \, dz = 0, \tag{55}$$

$$2\pi \int_{\text{SMC}} \left[\rho\left(w_s \partial_t^2 u_s + w_z \partial_t^2 u_z\right) + \lambda\left(\partial_s w_s + \partial_z w_z + s^{-1} w_s\right)\left(\partial_s u_s + \partial_z u_z + s^{-1} u_s\right)\right.$$

$$\left. + 2\mu\left(\partial_s w_s \partial_s u_s + \partial_z w_z \partial_z u_z + s^{-2} w_s u_s\right) + \mu\left(\partial_s w_z + \partial_z w_s\right)\left(\partial_s u_z + \partial_z u_s\right)\right] s \, ds \, dz$$

$$+ 2\pi \int_{\text{CMB}} \left(\frac{s w_s + z w_z}{\sqrt{s^2 + z^2}}\right)\partial_t^2 \chi \, s \, ds \, dz = \left\{\begin{array}{c} p_z \, w_z(0, r_\text{r}) \, \delta(t) \\ M_{zz} \, \partial_z w_z(0, r_\text{s}) \, H(t) \\ \frac{1}{2}(M_{xx} + M_{yy})\left[2\partial_s w_s(0, r_\text{s})\right] H(t) \end{array}\right\}. \tag{56}$$

As the braces in the final term indicate, eqs (54)–(56) are actually three independent coupled systems of equations, one for each of the three different types of monopole sources, p_z, M_{zz} and $\frac{1}{2}(M_{xx} + M_{yy})$. We present a detailed derivation of the $\frac{1}{2}(M_{xx} + M_{yy})$ axial source term $2\partial_s w_s$ in Appendix A.

4.6 Dipole source

We follow a similar 2-D reduction strategy in the case of a dipole source. From inspection of eqs (25)–(35), we can deduce that the solution $\mathbf{u}(\mathbf{r}, t)$, $\chi(\mathbf{r}, t)$ must be of the form

$$\mathbf{u} = [\hat{\mathbf{s}} u_s(s, z, t) + \hat{\mathbf{z}} u_z(s, z, t)]\cos\phi - \hat{\boldsymbol{\phi}} u_\phi(s, z, t)\sin\phi, \quad \chi = \chi(s, z, t)\cos\phi \tag{57}$$

in the case of either a p_x or M_{xz} source, and of the form

$$\mathbf{u} = [\hat{\mathbf{s}} u_s(s, z, t) + \hat{\mathbf{z}} u_z(s, z, t)]\sin\phi + \hat{\boldsymbol{\phi}} u_\phi(s, z, t)\cos\phi, \quad \chi = \chi(s, z, t)\sin\phi \tag{58}$$

in the case of either a p_y or M_{yz} source. As noted in Section 3.2, the response to a p_y or M_{yz} source at longitude ϕ is the same as the response to a p_x or M_{xz} source at longitude $\phi - \pi/2$, so that the functions u_s, u_z, u_ϕ are identical in eqs (57) and (58). It is also noteworthy that because of the factors $\cos\phi$ and $\sin\phi$, the symbols u_s, u_z, u_ϕ do not have their usual meaning (i.e. they are *not* the $\hat{\mathbf{s}}$, $\hat{\mathbf{z}}$, $\hat{\boldsymbol{\phi}}$ components of the

displacement $\mathbf{u}$). We again choose test functions $\mathbf{w}\,(\mathbf{r})$, $w(\mathbf{r})$ of the same form, namely

$$\mathbf{w} = [\hat{\mathbf{s}}\,w_s(s,z) + \hat{\mathbf{z}}\,w_z(s,z)]\cos\phi - \hat{\boldsymbol{\phi}}\,w_\phi(s,z)\sin\phi, \quad w = w(s,z)\cos\phi \tag{59}$$

or

$$\mathbf{w} = [\hat{\mathbf{s}}\,w_s(s,z) + \hat{\mathbf{z}}\,w_z(s,z)]\sin\phi + \hat{\boldsymbol{\phi}}\,w_\phi(s,z)\cos\phi, \quad w = w(s,z)\sin\phi, \tag{60}$$

substitute into the 3-D eqs (47)–(49), and evaluate the integrals, in this case, $\int_0^{2\pi}\cos^2\phi\,d\phi = \int_0^{2\pi}\sin^2\phi\,d\phi = \pi$ and $\int_0^{2\pi}\sin\phi\cos\phi\,d\phi = 0$, over the longitude ϕ. The resulting 2-D system of weak equations for a dipole source are

$$\int_{\text{SIC}}\Big\{\rho\big(w_s\partial_t^2 u_s + w_z\partial_t^2 u_z + w_\phi\partial_t^2 u_\phi\big) + \lambda\Big[\partial_s w_s + \partial_z w_z + s^{-1}(w_s - w_\phi)\Big]\Big[\partial_s u_s + \partial_z u_z + s^{-1}(u_s - u_\phi)\Big]$$

$$+ 2\mu\Big[\partial_s w_s\partial_s u_s + \partial_z w_z\partial_z u_z + s^{-2}(w_s - w_\phi)(u_s - u_\phi)\Big] + \mu(\partial_s w_z + \partial_z w_s)(\partial_s u_z + \partial_z u_s)$$

$$+ \mu\Big[\partial_s w_\phi + s^{-1}(w_s - w_\phi)\Big]\Big[\partial_s u_\phi + s^{-1}(u_s - u_\phi)\Big] + \mu(\partial_z w_\phi + s^{-1}w_s)(\partial_z u_\phi + s^{-1}u_s)\Big\}s\,ds\,dz$$

$$- \int_{\text{ICB}}\left(\frac{sw_s + zw_z}{\sqrt{s^2 + z^2}}\right)\partial_t^2\chi\,s\,ds\,dz = 0, \tag{61}$$

$$\int_{\text{FOC}}\Big[\kappa^{-1}w\partial_t^2\chi + \rho^{-1}(\partial_s w\partial_s\chi + \partial_z w\partial_z\chi + s^{-2}w\chi)\Big]s\,ds\,dz$$

$$+ \int_{\text{ICB}}w\left(\frac{su_s + zu_z}{\sqrt{s^2 + z^2}}\right)s\,ds\,dz - \int_{\text{CMB}}w\left(\frac{su_s + zu_z}{\sqrt{s^2 + z^2}}\right)s\,ds\,dz = 0, \tag{62}$$

$$\pi\int_{\text{SMC}}\Big\{\rho\big(w_s\partial_t^2 u_s + w_z\partial_t^2 u_z + w_\phi\partial_t^2 u_\phi\big) + \lambda\Big[\partial_s w_s + \partial_z w_z + s^{-1}(w_s - w_\phi)\Big]\Big[\partial_s u_s + \partial_z u_z + s^{-1}(u_s - u_\phi)\Big]$$

$$+ 2\mu\Big[\partial_s w_s\partial_s u_s + \partial_z w_z\partial_z u_z + s^{-2}(w_s - w_\phi)(u_s - u_\phi)\Big] + \mu(\partial_s w_z + \partial_z w_s)(\partial_s u_z + \partial_z u_s)$$

$$+ \mu\Big[\partial_s w_\phi + s^{-1}(w_s - w_\phi)\Big]\Big[\partial_s u_\phi + s^{-1}(u_s - u_\phi)\Big] + \mu(\partial_z w_\phi + s^{-1}w_z)(\partial_z u_\phi + s^{-1}u_z)\Big\}s\,ds\,dz$$

$$+ \pi\int_{\text{CMB}}\left(\frac{sw_s + zw_z}{\sqrt{s^2 + z^2}}\right)\partial_t^2\chi\,s\,ds\,dz = \left\{\begin{array}{c}(p_x\text{ or }p_y)\,w_+(0, r_\text{r})\,\delta(t) \\ (M_{xz}\text{ or }M_{yz})\Big[\partial_s w_z(0, r_\text{s}) + \partial_z w_+(0, r_\text{s})\Big]H(t)\end{array}\right\}, \tag{63}$$

where we have defined the auxiliary test functions

$$w_\pm(s,z) = \tfrac{1}{2}[w_s(s,z) \pm w_\phi(s,z)]. \tag{64}$$

We need only solve the 2-D weak eqs (61)–(63) once to find the response (57) to a p_x or M_{xz} source and the response (58) to a p_y or M_{yz} source. The p_x, p_y and M_{xz}, M_{yz} axial source terms w_+ and $\partial_s w_z + \partial_z w_+$ are derived in Appendix A.

4.7 Quadrupole source

The response $\mathbf{u}\,(\mathbf{r}, t)$, $\chi(\mathbf{r}, t)$ to a quadrupolar $\tfrac{1}{2}(M_{xx} - M_{yy})$ source is of the form

$$\mathbf{u} = [\hat{\mathbf{s}}\,u_s(s,z,t) + \hat{\mathbf{z}}\,u_z(s,z,t)]\cos 2\phi - \hat{\boldsymbol{\phi}}\,u_\phi(s,z,t)\sin 2\phi, \quad \chi = \chi(s,z,t)\cos 2\phi, \tag{65}$$

whereas the response to an M_{xy} source is of the form

$$\mathbf{u} = [\hat{\mathbf{s}}\,u_s(s,z,t) + \hat{\mathbf{z}}\,u_z(s,z,t)]\sin 2\phi + \hat{\boldsymbol{\phi}}\,u_\phi(s,z,t)\cos 2\phi, \quad \chi = \chi(s,z,t)\sin 2\phi. \tag{66}$$

Choosing test functions $\mathbf{w}\,(\mathbf{r})$, $w(\mathbf{r})$ of the same form, either

$$\mathbf{w} = [\hat{\mathbf{s}}\,w_s(s,z) + \hat{\mathbf{z}}\,w_z(s,z)]\cos 2\phi - \hat{\boldsymbol{\phi}}w_\phi(s,z)\sin 2\phi, \quad w = w(s,z)\cos 2\phi \tag{67}$$

or

$$\mathbf{w} = [\hat{\mathbf{s}}w_s(s,z) + \hat{\mathbf{z}}w_z(s,z)]\sin 2\phi + \hat{\boldsymbol{\phi}}\,w_\phi(s,z)\cos 2\phi, \quad w = w(s,z)\sin 2\phi, \tag{68}$$

and making use of the longitudinal identities $\int_0^{2\pi} \cos^2 2\phi \, d\phi = \int_0^{2\pi} \sin^2 2\phi \, d\phi = \pi$ and $\int_0^{2\pi} \sin 2\phi \cos 2\phi \, d\phi = 0$, we obtain the 2-D weak system of equations governing a quadrupole source:

$$\int_{\text{SIC}} \left\{ \rho \left(w_s \partial_t^2 u_s + w_z \partial_t^2 u_z + w_\phi \partial_t^2 u_\phi \right) + \lambda \left[\partial_s w_s + \partial_z w_z + s^{-1}(w_s - 2w_\phi) \right] \left[\partial_s u_s + \partial_z u_z + s^{-1}(u_s - 2u_\phi) \right] \right.$$
$$+ 2\mu \left[\partial_s w_s \partial_s u_s + \partial_z w_z \partial_z u_z + s^{-2}(w_s - 2w_\phi)(u_s - 2u_\phi) \right] + \mu (\partial_s w_z + \partial_z w_s)(\partial_s u_z + \partial_z u_s)$$
$$\left. + \mu \left[\partial_s w_\phi + s^{-1}(2w_s - w_\phi) \right] \left[\partial_s u_\phi + s^{-1}(2u_s - u_\phi) \right] + \mu (\partial_z w_\phi + 2s^{-1} w_s)(\partial_z u_\phi + 2s^{-1} u_s) \right\} s \, ds \, dz$$
$$- \int_{\text{ICB}} \left(\frac{s w_s + z w_z}{\sqrt{s^2 + z^2}} \right) \partial_t^2 \chi \, s \, ds \, dz = 0. \tag{69}$$

$$\int_{\text{FOC}} \left[\kappa^{-1} w \partial_t^2 \chi + \rho^{-1} (\partial_s w \partial_s \chi + \partial_z w \partial_z \chi + 4s^{-2} w \chi) \right] s \, ds \, dz$$
$$+ \int_{\text{ICB}} w \left(\frac{s u_s + z u_z}{\sqrt{s^2 + z^2}} \right) s \, ds \, dz - \int_{\text{CMB}} w \left(\frac{s u_s + z u_z}{\sqrt{s^2 + z^2}} \right) s \, ds \, dz = 0, \tag{70}$$

$$\int_{\text{SMC}} \left\{ \rho \left(w_s \partial_t^2 u_s + w_z \partial_t^2 u_z + w_\phi \partial_t^2 u_\phi \right) + \lambda \left[\partial_s w_s + \partial_z w_z + s^{-1}(w_s - 2w_\phi) \right] \left[\partial_s u_s + \partial_z u_z + s^{-1}(u_s - 2u_\phi) \right] \right.$$
$$+ 2\mu \left[\partial_s w_s \partial_s u_s + \partial_z w_z \partial_z u_z + s^{-2}(w_s - 2w_\phi)(u_s - 2u_\phi) \right] + \mu (\partial_s w_z + \partial_z w_s)(\partial_s u_z + \partial_z u_s)$$
$$\left. + \mu \left[\partial_s w_\phi + s^{-1}(2w_s - w_\phi) \right] \left[\partial_s u_\phi + s^{-1}(2u_s - u_\phi) \right] + \mu (\partial_z w_\phi + 2s^{-1} w_z)(\partial_z u_\phi + 2s^{-1} u_z) \right\} s \, ds \, dz$$
$$- \pi \int_{\text{ICB}} \left(\frac{s w_s + z w_z}{\sqrt{s^2 + z^2}} \right) \partial_t^2 \chi \, s \, ds \, dz = \left[\tfrac{1}{2}(M_{xx} - M_{yy}) \text{ or } M_{xy} \right] \left[2\partial_s w_+(0, r_s) \right] H(t). \tag{71}$$

Once again, we relegate the derivation of the source term $2\partial_s w_+$ to Appendix A.

4.8 Axial boundary conditions

Solutions $u_s(s, z, t)$, $u_z(s, z, t)$, $u_\phi(s, z, t)$, $\chi(s, z, t)$ to the weak eqs (54)–(56), (61)–(63) and (69)–(71) automatically satisfy the stress-free condition $\hat{\mathbf{r}} \cdot \mathbf{T} = \mathbf{0}$ on the semicircular right segment of the computational boundary $\partial\Omega$. Special attention must, however, be paid to the straight left segment of $\partial\Omega$, since it is a boundary of the 2-D computational domain Ω that does not have a physical counterpart in the 3-D earth model $\oplus$. The boundary conditions along this $s \to 0$ axis can be readily deduced by considering the $\theta \to 0$ limit of the mode-sum solution (25)–(35). The limiting behaviours of the associated Legendre equations in eqs (28) and (34) are (Dahlen & Tromp 1998, eq. B.62)

$$P_{l0}(\cos\theta) \sim 1, \quad P_{l1}(\cos\theta) \sim \tfrac{1}{2}l(l+1)\theta, \quad P_{l2}(\cos\theta) \sim \tfrac{1}{2}l(l+1)(l+2)(l-1)\theta^2. \tag{72}$$

The asymptotic functional form of the unknown variables u_s, u_z, u_ϕ, χ and associated test functions w_s, w_z, w_ϕ, w in the axial limit depends upon the source type:

p_z, M_{zz} or $\tfrac{1}{2}(M_{xx} + M_{yy})$ monopole source:

$$u_z \sim f(z, t), \quad u_s \sim f(z, t)s, \quad \chi \sim f(z, t), \tag{73}$$

$$w_z \sim f(z), \quad w_s \sim f(z)s, \quad w \sim f(z), \tag{74}$$

p_x, p_y or M_{xz}, M_{yz} dipole source:

$$u_+ \sim f(z, t), \quad u_z \sim f(z, t)s, \quad u_- \sim f(z, t)s^2, \quad \chi \sim f(z, t)s, \tag{75}$$

$$w_+ \sim f(z), \quad w_z \sim f(z)s, \quad w_- \sim f(z)s^2, \quad w \sim f(z)s, \tag{76}$$

$\tfrac{1}{2}(M_{xx} - M_{yy})$ or M_{xy} quadrupole source:

$$u_+ \sim f(z, t)s, \quad u_z \sim f(z, t)s^2, \quad u_- \sim f(z, t)s^3, \quad \chi \sim f(z, t)s, \tag{77}$$

$$w_+ \sim f(z)s, \quad w_z \sim f(z)s^2, \quad w_- \sim f(z)s^3, \quad w \sim f(z)s, \tag{78}$$

where, by analogy with eq. (64), we have defined

$$u_\pm(s, z, t) = \tfrac{1}{2}[u_s(s, z, t) \pm u_\phi(s, z, t)]. \tag{79}$$

The $s \to 0$ asymptotic properties (74), (76) and (78) of w_z and $w_\pm = \tfrac{1}{2}(w_s \pm w_\phi)$ have been used in Appendix A to evaluate the various source terms in eqs (56), (63) and (71).

Similar axial considerations arise in the application of the Fourier-spectral element method to the Navier–Stokes equations governing fluid flows in axisymmetric geometries (Lopez & Shen 1998; Lopez *et al.* 2002; Fournier *et al.* 2004, 2005). As in that fluid-dynamical context,

it is important to distinguish the so-called *essential* axial boundary conditions, which are all of Dirichlet type and must be specifically imposed in using a Galerkin formulation such as the spectral-element method (Karniadakis & Sherwin 1999) to solve the 2-D weak equations, from the Neumann and other higher-order boundary conditions (termed *natural*), which simply describe the expected asymptotic behaviour of the numerical solution and are implicitly satisfied. The essential $s \rightarrow 0$ boundary conditions for the three different source types are

$$p_z, M_{zz} \text{ or } \tfrac{1}{2}(M_{xx} + M_{yy}) \text{ monopole source:} \quad u_s = w_s = 0, \tag{80}$$

$$p_x, p_y \text{ or } M_{xz}, M_{yz} \text{ dipole source:} \quad u_z = u_- = w_z = w_- = 0, \chi = w = 0, \tag{81}$$

$$\tfrac{1}{2}(M_{xx} - M_{yy}) \text{ or } M_{xy} \text{ quadrupole source:} \quad u_z = u_\pm = w_z = w_\pm = 0, \chi = w = 0. \tag{82}$$

The Dirichlet conditions (80)–(82) must be imposed by axial masking of the unknowns $u_z, u_\pm, \chi$ and test functions $w_z, w_\pm, w$ in solving eqs (54)–(56), (61)–(63) and (69)–(71).

5 CONCLUSIONS

The principle of elastodynamic reciprocity enables the Fréchet sensitivity kernel for a seismic waveform to be computed by temporal and spatial differentiation, followed by convolution, of two unperturbed wavefields: the forward-propagating displacement response $\vec{\mathbf{u}}(\mathbf{r}, t)$ to a moment-tensor $\mathbf{M}H(t)$ at the source $\mathbf{r}_s$ and the backward-propagating response $\overleftarrow{\mathbf{u}}(\mathbf{r}, t)$ to a point force $\hat{\mathbf{p}}\,\delta(t)$ at the receiver $\mathbf{r}_r$. In this paper, we have described a divide-and-conquer strategy for computing the two responses $\vec{\mathbf{u}}(\mathbf{r}, t)$ and $\overleftarrow{\mathbf{u}}(\mathbf{r}, t)$ at all points $\mathbf{r}$ within a 3-D spherically symmetric earth by solving six systems of coupled weak equations within a planar, 2-D semicircular domain to account for all possible monopole, dipole and quadrupole, moment-tensor and point-force source types. The full 3-D responses $\vec{\mathbf{u}}(\mathbf{r}, t)$ and $\overleftarrow{\mathbf{u}}(\mathbf{r}, t)$ can be reconstructed from the six 2-D solutions, together with the known azimuthal dependence of the waves excited by the various sources. These results establish the foundation for the paper that follows (Nissen-Meyer *et al.* 2007), in which we develop and implement a spectral-element method to solve the resulting 2-D weak equations. Our ultimate objective is the development of a flexible and efficient scheme for computing spherical-earth, finite-frequency sensitivity kernels for arbitrary seismic phases and source–receiver configurations, with an initial focus upon waves that probe the highly heterogeneous and geodynamically interesting D″ region above the Earth's core–mantle boundary.

ACKNOWLEDGMENTS

REFERENCES

Aki, K. & Richards, P., 1980. *Quantitative Seismology: Theory and Methods*, W.H. Freeman & Co., San Francisco, California.

Bernardi, C., Dauge, M. & Maday, Y., 1999. *Spectral Methods for Axisymmetric Domains*, Vol. 3 of Series in Applied Mathematics, Gauthier-Villars, Paris, Numerical algorithms and tests by Mejdi Azaïez.

Capdeville, Y., 2005. An efficient Born normal mode method to compute sensitivity kernels and synthetic seismograms in the earth, *Geophys. J. Int.,* **163**, 639–646.

Chaljub, E. & Tarantola, A., 1997. Sensitivity of SS precursors to topography on the upper-mantle 660 km discontinuity, *Geophys. Res. Lett.,* **24**, 2613–2616.

Chaljub, E. & Valette, B., 2004. Spectral element modeling of three dimensional wave propagation in a self-gravitating Earth with an arbitrarily stratified outer core, *Geophys. J. Int.,* **158**, 131–141.

Chapman, C., 2004. *Fundamentals of Seismic Wave Propagation*, Cambridge University Press, Cambridge.

Dahlen, F.A., 2005. Finite-frequency sensitivity kernels for boundary topography perturbations, *Geophys. J. Int.,* **162**, 525–540.

Dahlen, F.A. & Baig, A., 2002. Fréchet kernels for body wave amplitudes, *Geophys. J. Int.,* **150**, 440–466.

Dahlen, F.A. & Tromp, J., 1998. *Theoretical Global Seismology*, Princeton University Press, Princeton, New Jersey.

Dahlen, F.A., Hung, S.-H. & Nolet, G., 2000. Fréchet kernels for finite-frequency traveltimes—I. Theory, *Geophys. J. Int.,* **141**, 175–203.

Davaille, A., 1999. Simultaneous generation of hotspots and superswells by convection in a heterogenous planetary mantle, *Nature,* **402**, 756–760.

Dziewonski, A. & Anderson, D., 1981. Preliminary Reference Earth Model, *Phys. Earth planet. Inter.,* **25**, 297–356.

Favier, N. & Chevrot, S., 2003. Sensitivity kernels for shear wave splitting in transverse isotropic media, *Geophys. J. Int.,* **153**, 213–228.

Fournier, A., Bunge, H.-P., Hollerbach, R. & Vilotte, J.-P., 2004. Application of the spectral element method to the axisymmetric Navier-Stokes equation, *Geophys. J. Int.,* **156**, 682–700.

Fournier, A., Bunge, H.-P., Hollerbach, R. & Vilotte, J.-P., 2005. A Fourier-spectral element algorithm for thermal convection in rotating axisymmetric containers, *J. Comp. Phys.,* **204**, 462–489.

Gauthier, O., Virieux, J. & Tarantola, A., 1986. Two-dimensional nonlinear inversion of seismic waveforms—numerical results, *Geophysics,* **51**, 1387–1403.

Gerritsma, M. & Phillips, T., 2000. Spectral element methods for axisymmetric Stokes problems, *J. Comp. Phys.,* **164**, 81–103.

Gu, Y.J., Dziewonski, A.M. & Ekström, G., 2003. Simultaneous inversion for mantle shear velocity and topography of transition zone discontinuities, *Geophys. J. Int.,* **154**, 559–583.

Hung, S.-H., Garnero, E., Chiao, L.-Y., Kuo, B.-Y. & Lay, T., 2005. Finite-frequency tomography of D″ shear velocity heterogeneity beneath the Caribbean, *J. geophys. Res.,* **110**, doi:10.1029/2004JB003373.

Igel, H. & Weber, M., 1995. SH-wave propagation in the whole mantle using high-order finite differences, *Geophys. Res. Lett.,* **22**, 731–734.

Igel, H. & Weber, M., 1996. P-SV wave propagation in the Earth's mantle using finite differences: application to heterogeneous lowermost mantle structure, *Geophys. Res. Lett.,* **23**, 415–418.

Ishii, M., Dziewonski, A.M., Tromp, J. & Ekström, G., 2002. Joint inversion of normal-mode and body-wave data for inner-core anisotropy: 2. Possible complexities, *J. geophys. Res.,* **107**, doi:10.1029/2001JB000713.

Karniadakis, G.E. & Sherwin, S.J., 1999. *Spectral/hp Element Methods for CFD*, Oxford University Press, Oxford.

Kellogg, L.H., Hager, B.H. & van der Hilst, R.H., 1999. Compositional stratification in the deep mantle, *Science,* **283,** 1881–1884.

Kendall, J.-M., 2000. Seismic anisotropy in the boundary layers of the Earth's mantle, in *Earth's Deep Interior: Mineral Physics and Tomography from the Atomic to the Global Scale*, pp. 149–175, eds Karato, S., Stixrude, L., Liebermann, R.C., Masters, T.G. & Forte, A.M., Geophysical Monograph Series 117, American Geophysical Union.

Komatitsch, D. & Tromp, J., 2002. Spectral-element simulations of global seismic wave propagation—I. Validation, *Geophys. J. Int.,* **149,** 390–412.

Komatitsch, D., Barnes, C. & Tromp, J., 2000. Wave propagation near a fluid-solid interface: A spectral element approach, *Geophysics,* **65,** 623–631.

Lay, T. & Garnero, E., 2004. Core-mantle boundary structures and processes, in *The State of the Planet: Frontiers and Challenges in Geophysics*, eds Sparks, R.S.J. & Hawkesworth, C.J., Geophysical Monograph 150, IUGG Volume 19, doi:10.1029/150GM04.

Lay, T., Garnero, E. & Williams, Q., 2004. Partial melting in a thermo-chemical boundary layer at the base of the mantle, *Phys. Earth planet. Inter.,* **146,** 441–467.

Lopez, J. & Shen, J., 1998. An efficient spectral-projection method for the Navier-Stokes equations in cylindrical geometries I. Axisymmetric cases, *J. Comp. Phys.,* **139,** 308–326.

Lopez, J., Marques, F. & Shen, J., 2002. An efficient spectral-projection method for the Navier-Stokes equations in cylindrical geometries II. Three dimensional cases, *J. Comp. Phys.,* **176,** 384–401.

Luo, Y. & Schuster, G., 1991. Wave equation traveltime inversion, *Geophysics,* **56,** 645–653.

Marquering, H., Nolet, G. & Dahlen, F.A., 1998. Three-dimensional waveform sensitivity kernels, *Geophys. J. Int.,* **132,** 521–534.

Montelli, R., Nolet, G., Dahlen, F.A., Masters, G., Engdahl, E.R. & Hung, S.-H., 2004. Finite-frequency tomography reveals a variety of plumes in the mantle, *Science,* **303,** 338–343.

Ni, S., Helmberger, D. & Tromp, J., 2005. Three-dimensional structure of the african superplume from waveform modelling, *Geophys. J. Int.,* **161,** 283–294.

Nissen-Meyer, T., Fournier, A. & Dahlen, F.A., 2007. A two-dimensional spectral-element method for computing spherical-earth seismograms – I. Moment-tensor source, *Geophys. J. Int.,* doi:10.1111/j.1365-246X.2006.03121.x.

Rost, S., Garnero, E., Williams, Q. & Manga, M., 2005. Seismic constraints on a possible plume root at the core-mantle boundary, *Nature,* **435,** 666–669.

Tarantola, A., 1984. Inversion of seismic reflection data in the acoustic approximation, *Geophysics,* **49,** 1259–1266.

To, A., Romanowicz, B., Capdeville, Y. & Takeuchi, N., 2005. 3D effects of sharp boundaries at the borders of the African and Pacific Superplumes: observation and modeling, *Earth planet. Sci. Lett.,* **233,** 137–153.

Tromp, J., Tape, C. & Liu, Q., 2005. Seismic tomography, adjoint methods, time reversal and banana-doughnut kernels, *Geophys. J. Int.,* **160,** 195–216.

Woodhouse, J.H. & Dahlen, F.A., 1978. The effect of a general aspherical perturbation on the free oscillations of the Earth, *Geophys. J. R. astr. Soc.,* **53,** 335–354.

Woodward, M.J., 1992. Wave-equation tomography, *Geophysics,* **57,** 15–26.

Yu, W.-C., Wen, L. & Niu, F., 2005. Seismic velocity structure in the Earth's outer core, *J. geophys. Res.,* **110,** doi:10.1029/2003JB002928.

Zhao, L., Jordan, T. & Chapman, C.H., 2000. Three-dimensional Fréchet differential kernels for seismic delay times, *Geophys. J. Int.,* **141,** 558–576.

Zhao, L., Jordan, T., Olsen, K.B. & Chen, P., 2005. Fréchet kernels for imaging regional earth structure based on three-dimensional reference models, *Bull. seism. Soc. Am.,* **95,** 2066–2080.

Zhou, Y., Dahlen, F.A. & Nolet, G., 2004. 3-D sensitivity kernels for surface-wave observables, *Geophys. J. Int.,* **158,** 142–168.

APPENDIX A: DERIVATION OF THE AXIAL SOURCE TERMS

The 2-D systems of weak eqs (54)–(56), (61)–(63) and (69)–(71) are noteworthy in that they enable synthetic-seismogram computations for a point-force or moment-tensor source $\hat{\mathbf{p}}\,\delta(\mathbf{r}-\mathbf{r}_r)\,\delta(t)$ or $-\mathbf{M}:\nabla\,\delta(\mathbf{r}-\mathbf{r}_s)\,H(t)$ situated on the axis $s=0$. In contrast, only a monopole source, including a toroidal ring source artificially situated one grid point away from the axis, can be treated using a 2-D, axisymmetric finite-difference method based upon the strong form (Chaljub & Tarantola 1997; Igel & Weber 1995, 1996). Since the successful incorporation of a point-force or moment-tensor source is the principal advantage of the present 2-D formulation, and since the source terms in eqs (56), (63) and (71) depend upon a systematic application of the axial boundary conditions (73)–(78), we present a detailed derivation here. All of the test functions w_z, w_s, w_ϕ and $w_\pm = \frac{1}{2}(w_s \pm w_\phi)$ in this appendix are evaluated on the axis, at either the receiver point $\mathbf{r}_r = (r_r, 0, \cdot)$ or the source point $\mathbf{r}_s = (r_s, 0, \cdot)$.

A1 Monopole source

Both a p_z and a M_{zz} source are straightforward; the axial source terms are, respectively, w_z and $\partial_z w_z$. In the case of a $\frac{1}{2}(M_{xx} + M_{yy})$ source, the source term is $(\hat{\mathbf{x}}\hat{\mathbf{x}} + \hat{\mathbf{y}}\hat{\mathbf{y}}):\nabla\mathbf{w}$, where

$$\nabla\mathbf{w} = \hat{\mathbf{s}}\hat{\mathbf{s}}\,\partial_s w_w + \hat{\mathbf{z}}\hat{\mathbf{z}}\,\partial_z w_z + \hat{\boldsymbol{\phi}}\hat{\boldsymbol{\phi}}\,s^{-1}w_s + \hat{\mathbf{s}}\hat{\mathbf{z}}\,\partial_s w_z + \hat{\mathbf{z}}\hat{\mathbf{s}}\,\partial_z w_s. \tag{A1}$$

Utilizing the elementary transformation formulae $\hat{\mathbf{x}} = \hat{\mathbf{s}}\cos\phi - \hat{\boldsymbol{\phi}}\sin\phi$, $\hat{\mathbf{y}} = \hat{\mathbf{s}}\sin\phi + \hat{\boldsymbol{\phi}}\cos\phi$, we obtain

$$(\hat{\mathbf{x}}\hat{\mathbf{x}} + \hat{\mathbf{y}}\hat{\mathbf{y}}):\nabla\mathbf{w} = (\partial_s w_s + s^{-1}w_s)(\cos^2\phi + \sin^2\phi) = 2\partial_s w_s, \tag{A2}$$

where we have used the axial boundary condition $\partial_s w_s = s^{-1}\,w_s$, which is equivalent to the second of eqs (74), to obtain the final relation.

A2 Dipole source

The source term for a p_x dipole source is

$$\hat{\mathbf{x}}\cdot\mathbf{w} = (\hat{\mathbf{s}}\cos\phi - \hat{\boldsymbol{\phi}}\sin\phi)\cdot[(\hat{\mathbf{s}}\,w_s + \hat{\mathbf{z}}\,w_z)\cos\phi - \hat{\boldsymbol{\phi}}\,w_\phi\sin\phi]$$

$$= w_s\cos^2\phi + w_\phi\sin^2\phi = w_+(\cos^2\phi + \sin^2\phi) + w_-(\cos^2\phi - \sin^2\phi)$$

$$= w_+, \tag{A3}$$

where we have used the axial boundary condition $w_- = 0$. The source term for a p_y source is

$$
\begin{aligned}
\hat{\mathbf{y}} \cdot \mathbf{w} &= (\hat{\mathbf{s}} \sin\phi + \hat{\boldsymbol{\phi}} \cos\phi) \cdot [(\hat{\mathbf{s}}\, w_s + \hat{\mathbf{z}}\, w_z) \sin\phi + \hat{\boldsymbol{\phi}}\, w_\phi \cos\phi] \\
&= w_s \sin^2\phi + w_\phi \cos^2\phi = w_+(\sin^2\phi + \cos^2\phi) + w_-(\sin^2\phi - \cos^2\phi) \\
&= w_+,
\end{aligned}
\tag{A4}
$$

which is identical to eq. (A3), as expected. The source term for an M_{xz} dipole source is $(\hat{\mathbf{x}}\hat{\mathbf{z}} + \hat{\mathbf{z}}\hat{\mathbf{x}}) : \nabla\mathbf{w}$, where

$$
\begin{aligned}
\nabla\mathbf{w} = {}& [\hat{\mathbf{s}}\hat{\mathbf{s}}\, \partial_s w_s + \hat{\mathbf{z}}\hat{\mathbf{z}}\, \partial_z w_z + \hat{\boldsymbol{\phi}}\hat{\boldsymbol{\phi}}\, s^{-1}(w_s - w_\phi) + \hat{\mathbf{s}}\hat{\mathbf{z}}\, \partial_s w_z + \hat{\mathbf{z}}\hat{\mathbf{s}}\, \partial_z w_s] \cos\phi \\
&- [\hat{\mathbf{s}}\hat{\boldsymbol{\phi}}\, \partial_s w_\phi + \hat{\boldsymbol{\phi}}\hat{\mathbf{s}}\, s^{-1}(w_s - w_\phi) + \hat{\mathbf{z}}\hat{\boldsymbol{\phi}}\, \partial_z w_\phi + \hat{\boldsymbol{\phi}}\hat{\mathbf{z}}\, s^{-1} w_z] \sin\phi.
\end{aligned}
\tag{A5}
$$

Utilizing $\hat{\mathbf{x}} = \hat{\mathbf{s}} \cos\phi - \hat{\boldsymbol{\phi}} \sin\phi$, we obtain

$$
\begin{aligned}
(\hat{\mathbf{x}}\hat{\mathbf{z}} + \hat{\mathbf{z}}\hat{\mathbf{x}}) : \nabla\mathbf{w} &= (\partial_s w_z + \partial_z w_s)\cos^2\phi + (s^{-1} w_z + \partial_z w_\phi)\sin^2\phi \\
&= \tfrac{1}{2}(\partial_s w_z + s^{-1} w_z + 2\partial_z w_+)(\cos^2\phi + \sin^2\phi) + \tfrac{1}{2}(\partial_s w_z - s^{-1} w_z + 2\partial_z w_-)(\cos^2\phi - \sin^2\phi) \\
&= \partial_s w_z + \partial_z w_+,
\end{aligned}
\tag{A6}
$$

where we have used the axial boundary conditions $\partial_z w_z = s^{-1} w_z$ and $w_- = 0$. The source term for an M_{yz} source is $(\hat{\mathbf{y}}\hat{\mathbf{z}} + \hat{\mathbf{z}}\hat{\mathbf{y}}) : \nabla\mathbf{w}$, where

$$
\begin{aligned}
\nabla\mathbf{w} = {}& [\hat{\mathbf{s}}\hat{\mathbf{s}}\, \partial_s w_s + \hat{\mathbf{z}}\hat{\mathbf{z}}\, \partial_z w_z + \hat{\boldsymbol{\phi}}\hat{\boldsymbol{\phi}}\, s^{-1}(w_s - w_\phi) + \hat{\mathbf{s}}\hat{\mathbf{z}}\, \partial_s w_z + \hat{\mathbf{z}}\hat{\mathbf{s}}\, \partial_z w_s] \sin\phi \\
&+ [\hat{\mathbf{s}}\hat{\boldsymbol{\phi}}\, \partial_s w_\phi + \hat{\boldsymbol{\phi}}\hat{\mathbf{s}}\, s^{-1}(w_s - w_\phi) + \hat{\mathbf{z}}\hat{\boldsymbol{\phi}}\, \partial_z w_\phi + \hat{\boldsymbol{\phi}}\hat{\mathbf{z}}\, s^{-1} w_z] \cos\phi.
\end{aligned}
\tag{A7}
$$

Utilizing $\hat{\mathbf{y}} = \hat{\mathbf{s}} \sin\phi + \hat{\boldsymbol{\phi}} \cos\phi$, we obtain

$$
\begin{aligned}
(\hat{\mathbf{y}}\hat{\mathbf{z}} + \hat{\mathbf{z}}\hat{\mathbf{y}}) : \nabla\mathbf{w} &= (\partial_s w_z + \partial_z w_s)\sin^2\phi + (s^{-1} w_z + \partial_z w_\phi)\cos^2\phi \\
&= \frac{1}{2}(\partial_s w_z + s^{-1} w_z + 2\partial_z w_+)(\sin^2\phi + \cos^2\phi) + \tfrac{1}{2}(\partial_s w_z - s^{-1} w_z + 2\partial_z w_-)(\sin^2\phi - \cos^2\phi) \\
&= \partial_s w_z + \partial_z w_+,
\end{aligned}
\tag{A8}
$$

which is identical to eq. (A6).

A3 Quadrupole source

The axial source term for a $\frac{1}{2}(M_{xx} - M_{yy})$ quadrupole source is $(\hat{\mathbf{x}}\hat{\mathbf{x}} - \hat{\mathbf{y}}\hat{\mathbf{y}}) : \nabla\mathbf{w}$, where

$$
\begin{aligned}
\nabla\mathbf{w} = {}& [\hat{\mathbf{s}}\hat{\mathbf{s}}\, \partial_s w_s + \hat{\mathbf{z}}\hat{\mathbf{z}}\, \partial_z w_z + \hat{\boldsymbol{\phi}}\hat{\boldsymbol{\phi}}\, s^{-1}(w_s - 2w_\phi) + \hat{\mathbf{s}}\hat{\mathbf{z}}\, \partial_s w_z + \hat{\mathbf{z}}\hat{\mathbf{s}}\, \partial_z w_s] \cos 2\phi \\
&- [\hat{\mathbf{s}}\hat{\boldsymbol{\phi}}\, \partial_s w_\phi + \hat{\boldsymbol{\phi}}\hat{\mathbf{s}}\, s^{-1}(2w_s - w_\phi) + \hat{\mathbf{z}}\hat{\boldsymbol{\phi}}\, \partial_z w_\phi + \hat{\boldsymbol{\phi}}\hat{\mathbf{z}}\, (2s^{-1} w_z)] \sin 2\phi.
\end{aligned}
\tag{A9}
$$

Utilizing $\hat{\mathbf{x}} = \hat{\mathbf{s}} \cos\phi - \hat{\boldsymbol{\phi}} \sin\phi$ and $\hat{\mathbf{y}} = \hat{\mathbf{s}} \sin\phi + \hat{\boldsymbol{\phi}} \cos\phi$, we obtain

$$
\begin{aligned}
(\hat{\mathbf{x}}\hat{\mathbf{x}} - \hat{\mathbf{y}}\hat{\mathbf{y}}) : \nabla\mathbf{w} &= [\partial_s w_s - s^{-1}(w_s - 2w_\phi)]\cos^2 2\phi + [\partial_s w_\phi + s^{-1}(2w_s - w_\phi)]\sin^2 2\phi \\
&= (\partial_s w_+ + s^{-1} w_+)(\cos^2 2\phi + \sin^2 2\phi) + (\partial_s w_- - 3s^{-1} w_-)(\cos^2 2\phi - \sin^2 2\phi) \\
&= 2\partial_s w_+,
\end{aligned}
\tag{A10}
$$

where we have used the axial boundary conditions $\partial_s w_+ - s^{-1} w_+ = 0$ and $\partial_s w_- - 3s^{-1} w_-$, which are equivalent to the first and third of eqs (78). In the case of an M_{xy} source, eqs (A9) and (A10) are replaced by

$$
\begin{aligned}
\nabla\mathbf{w} = {}& [\hat{\mathbf{s}}\hat{\mathbf{s}}\, \partial_s w_s + \hat{\mathbf{z}}\hat{\mathbf{z}}\, \partial_z w_z + \hat{\boldsymbol{\phi}}\hat{\boldsymbol{\phi}}\, s^{-1}(w_s - 2w_\phi) + \hat{\mathbf{s}}\hat{\mathbf{z}}\, \partial_s w_z + \hat{\mathbf{z}}\hat{\mathbf{s}}\, \partial_z w_s] \sin 2\phi \\
&+ [\hat{\mathbf{s}}\hat{\boldsymbol{\phi}}\, \partial_s w_\phi + \hat{\boldsymbol{\phi}}\hat{\mathbf{s}}\, s^{-1}(2w_s - w_\phi) + \hat{\mathbf{z}}\hat{\boldsymbol{\phi}}\, \partial_z w_\phi + \hat{\boldsymbol{\phi}}\hat{\mathbf{z}}\, (2s^{-1} w_z)] \cos 2\phi
\end{aligned}
\tag{A11}
$$

and

$$
\begin{aligned}
(\hat{\mathbf{x}}\hat{\mathbf{x}} + \hat{\mathbf{y}}\hat{\mathbf{y}}) : \nabla\mathbf{w} &= [\partial_s w_s - s^{-1}(w_s - 2w_\phi)]\sin^2 2\phi + [\partial_s w_\phi + s^{-1}(2w_s - w_\phi)]\cos^2 2\phi \\
&= (\partial_s w_+ + s^{-1} w_+)(\sin^2 2\phi + \cos^2 2\phi) + (\partial_s w_- - 3s^{-1} w_-)(\sin^2 2\phi - \cos^2 2\phi) \\
&= 2\partial_s w_+,
\end{aligned}
\tag{A12}
$$

so that the $\frac{1}{2}(M_{xx} - M_{yy})$ and M_{xy} source terms are the same.

A4 Summary

In summary, the weak-form source terms for the six independent, 2-D problems listed in Section 3.2 are

  (i) a p_z monopole source: w_z,
  (ii) an M_{zz} monopole source: $\partial_z w_z$,
  (iii) a $\frac{1}{2}(M_{xx} + M_{yy})$ monopole source: $2\partial_s w_s$,

(iv) a p_x or p_y dipole source: w_s,

(v) an M_{xz} or M_{yz} dipole source: $\partial_s w_z + \partial_z w_+$,

(vi) a $\frac{1}{2}(M_{xx} - M_{yy})$ or M_{xy} quadrupole source: $2\partial_s w_+$.

Three axial derivatives arise: $\partial_s w_s$ in case (iii), $\partial_s w_z$ in case (v) and $\partial_s w_+$ in case (vi). In every instance, the differentiated quantity w_s, w_z or w_+ is the only variable that varies linearly with s in the vicinity of the axis.